nature portfolio

Peer Review File

Impact-Resistant Supercapacitor by Hydrogel-Infused Lattice

REVIEWER COMMENTS

Reviewer #1 (Remarks to the Author):

1. The novelty of this paper is limited. The authors claimed that hydrogel electrolyte infusion into 3D printed ceramic lattice electrodes enables impact resistant supercapacitors. Actually, sandwiching soft-hard materials into lamellar structures is a common strategy to generate toughened structural composites. And this strategy has also been applied to enhance the mechanical properties of energy storage devices even 10 years ago (e.g., Westover, Andrew S., et al. "A multifunctional load-bearing solid-state supercapacitor." Nano letters 14.6 (2014): 3197-3202.)

2. The authors have presented the fabrication of several SiOC lattices with varying TPMS architects as electrodes and separators. Although they look pretty fancy, I cannot see the rationality of these structures and why they are chosen here. Of course, different structured lattices will show different mechanical response under impact. However, I think even without these structures, the SiOC ceramic itself is strong enough to provide extraordinary mechanical properties. If you think these structures can provide high surface area for electrolyte infilling, I will say the feature size (a few hundred microns) of printed structures is too large and increasing surface roughness/nanopores are better way to enlarge the accessible areas. Therefore, I think the relationship between these 3D structured electrodes and the devices mechanical/electrochemical performance is not clear. Besides, the separators are also printed into TPMS structures. I don't think such complex architectured separators are necessary. I know 3D printing is a hot area, but don't abuse the additively manufactured structural materials.

3. The authors fabricated four types of TPMS lattices, Gyroid, Diamond, Primitive, and I-WP with different porosity, relative density, and surface area. I think that direct comparison of these devices mechanical properties and electrochemical performance is unreasonable since so many structural parameters are different. We cannot simply conclude which structure is the best. Besides, for the lattice structures, the scale effect is very important. If you increase the printing resolution, scaling law in Ashby map will be significantly different. Current resolution is too big for stereolithography-based 3D printing.

4. The advantage of supercapacitors is their high-power density, but their low energy density is always a problem that has hampered the real application. The authors used ceramic as electrode scaffolds that not only introduce complex post-processing procedures (conductive carbon and PANI coating), but also increase the dead weight to decrease the gravimetric energy density. This strategy cannot reconcile the mechanical strength and energy density. Besides, I'm not sure if SiO contributes any electrochemical capacitance. Please provide XPS analysis of Si before and after stability tests.

5. I also noticed that the integrated electrode, separator, and PVA hydrogel electrolyte are assembled into a FDM printed mold, as shown in Fig. 2a. That means you put an ultra-strong system into a weak container. Have you considered the whole system as a whole? Unless you make an impact resistant case, otherwise all works discussed in this paper are meaningless.

6. In comparison, the flexible supercapacitor is a better solution to achieve high impact tolerance and excellent electrochemical performance by combining flexible electrodes and gel electrolytes. (e.g., Yang, Yongrui, et al. "Recent progress in the all-solid-state flexible supercapacitors." SmartMat 3.3 (2022): 349-383.)

I don't think this paper is good enough to publish at NC and suggest rejecting it.

Reviewer #2 (Remarks to the Author):

Comments to the Author:
The manuscript (Manuscript Number: NCOMMS-24-13148, Title: Impact-Resistant Supercapacitor by Hydrogel-Infused Lattice) reports Impact-resistant and ready-to-use supercapacitors constructed from self-healable hydrogel electrolytes infused structurally reinforced lattice electrodes. Moreover, 3D-printed conductive C/SiOC current collectors provided superior mechanical protection. The designs and fabrication of the flexible supercapacitors are interesting. I will suggest the publication of the works after minor revision. Here are some questions:
1. Will the electrochemical performance of the supercapacitor attenuate after repeated twist and stretch.
2. On Page 23, The authors wrote: "Upon recontact, these cleaved bonds underwent reformation, facilitating the regeneration and self-repair of the crosslinked network (Fig. 3g and 5e)", please check the name of the Figure 3 (g) carefully.
3. The authors wrote: "The XRD pattern of PANI/C/SiOC displayed a small but sharp peak at 25.6°, corresponding to the (200) crystal planes of emeraldine salt (Fig. 1c)", but it is (220) crystal planes into Fig. 1c, Which one is correct.
4. The samples should be characterized by spectroscopic techniques after long cycling tests. The cycling stability experiments need to be performed again minimum for 5000 cycles.
5. Can authors compare the key material parameters of PANI/C/SiOC prepared in this work with the prior-art and other available materials for supercapacitor application?

Reviewer #3 (Remarks to the Author):

The authors described an impact-resistant and ready-to-use supercapacitors constructed from self-healable hydrogel electrolytes infused structurally reinforced lattice electrodes. The obtained supercapacitors exhibited good electrochemical performance with a static specific capacitance of 585.51 mF/cm3 at a current density of 3 mA/cm3. It maintained operational integrity under extreme conditions, including post-impact with energy of 0.3 J/cm3, dynamic loading ranging from 0 to 18.83 MPa, and self-healing after electrolyte damage. This approach provides a facile strategy for creating damage-invulnerable energy storage devices. The approach is systematic and the quality of the presentation in the manuscript is very good. However, the following points should be addressed before the manuscript can be accepted for publication.

1. The introduction states that "Supercapacitors, as burgeoning storage devices, are no exception. Their rapid charge-discharge rates make them apt for extreme environments". The logical correlation between the rapid charge-discharge rates of supercapacitors and their applicability to extreme environments is puzzling. It is therefore recommended that more precise wording be used.

2. A clearer description of the innovation of the study is suggested in the introduction section.

3. Some data should be measured several times and given as mean ± standard deviation, e.g. mechanical properties and conductivity.

4. The hydrogel electrolyte adheres to the electrode by in situ molding. Is it possible that mechanical interlocking due to the configuration design of the electrodes also contributes to the adhesion? This should be clarified.

5. The mechanical properties of the SIOC without surface-configuration design and its electrochemical performance after assembly into supercapacitors should be given for presenting the advantages of this work.

6. Why do Cell G and Cell P in Fig. 3g show differences in charging and discharging behavior with Cell D and Cell I-WP in the mid-charging and late discharging stages?

7. Abbreviations appear directly in some words, e.g., XPS, which authors are asked to double-check and revise.

From:

Jun DING, Professor, PhD

Department of Materials Science and Engineering

National University of Singapore, Singapore 117575

Tel: (65) 6516 4317; Fax: (65) 6776 3640

Email: msedingj@nus.edu.sg

6 May 2024

Dear Editors and Reviewers,

We are sincerely grateful for the opportunity to revise our manuscript to ***Nature Communications***. Our team extends profound appreciation to the editor and reviewers for their insightful and constructive comments regarding our manuscript titled "**Impact-Resistant Supercapacitor by Hydrogel-Infused Lattice**" (NCOMMS-24-13148).

We have meticulously reviewed and considered the comments provided by the editor and reviewers. In response to the detailed suggestions, we have undertaken a thorough revision of the original manuscript. For ease of review, all modifications have been highlighted in red in the revised submission, which we respectfully submit for your esteemed consideration.

Responses to Reviewers

Reviewer #1

1. The novelty of this paper is limited. The authors claimed that hydrogel electrolyte infusion into 3D printed ceramic lattice electrodes enables impact resistant supercapacitors. Actually, sandwiching soft-hard materials into lamellar structures is a common strategy to generate toughened structural

composites. And this strategy has also been applied to enhance the mechanical properties of energy storage devices even 10 years ago (e.g., Westover, Andrew S., et al. "A multifunctional load-bearing solid-state supercapacitor." Nano letters 14.6 (2014): 3197-3202.)

Response: Thank you for your valuable time and professional insights. We sincerely appreciate your criticisms and comments. Although soft-hard lamellar structures are commonly employed in toughened composites, our work introduces a different approach using a hydrogel-infused lattice structure with a continuous and periodic all-SiOC-based skeleton other than lamellar structures, which avoids the mechanical weak points typical of lamellar structures. Thus, our approach substantially differs from Westover's, despite sharing similar goals of enhancing the safety of energy storage devices. While the basic "electrode-electrolyte-electrode" configuration may appear similar in schematic representations, our work diverges significantly in terms of electrode and electrolyte materials, fabrication processes, assembly strategies, and energy storage mechanisms. Westover's research used porous silicon plates as electrodes with a PEO/$EMIBF_4$ solid-state electrolyte, assembled by vacuum infiltration and solidification, focusing on the tensile performance of the electrolyte. In contrast, our study employs 3D-printed C/SiOC as the current collector with a nanorod-PANI coating for pseudocapacitance, and a self-healable PVA hydrogel as the electrolyte, assembled via a freeze-thaw process. Consequently, while Westover's configuration functions as an electric double-layer capacitor, our PANI/C/SiOC cell functions as a pseudocapacitor, which is quite different. Moreover, our work emphasizes performance under dynamic pressure loads, post-impact, and after self-healing of the hydrogel electrolyte, aiming to develop a comprehensive and customized supercapacitor strategy while addressing safety concerns. The 3D printing technique enhances design flexibility, allowing for structurally optimized electrodes that improve space utilization and mechanical performance compared to traditional plate or film electrodes. This capability facilitates customized designs tailored to specific application requirements. Therefore, our research aims to provide a robust, damage-resistant supercapacitor strategy which can be promoted in other supercapacitor systems, rather than merely

enhancing load-bearing performance. Based on your feedback, we have added illustrations of the supercapacitor configuration and assembly manner in the introduction: "The assembly strategy of the supercapacitor cell is also crucial to mechanical stability. Given that supercapacitors employ an "electrode-electrolyte-electrode" configuration, they are typically constructed using lamellar structures. This arrangement may introduce mechanical weak points determined by the least robust component within the structure and induce anisotropy in mechanical behavior. To develop a mechanically coherent and isotropic supercapacitor cell, we employed a continuous all-SiOC-based skeleton to enhance mechanical performance uniformly. Triply periodic minimal surface (TPMS) configurations were used to construct the SiOC skeleton, leveraging their structural uniformity and periodicity. Electrodes were fabricated via in-situ growth of active materials on the TPMS-structured SiOC, paired with an insulating SiOC separator that shared the same TPMS design. The hydrogel electrolyte was infused into the hollow spaces to complete a hydrogel-infused TPMS lattice configuration as a ready-to-use supercapacitor cell." (Page 5, lines 3-15)

The difference from Westover's work was discussed to further underscore our study's novelty: "Since this design was reinforced by the continuous SiOC skeleton, weak phases and anisotropic mechanical behavior common in lamellar or sandwich structures can be avoided. This uniform continuity and periodicity between the electrode and separator allowed the skeleton to distribute stress evenly, mitigating stress concentration. Furthermore, the employment of scalable and customizable 3D printing techniques endowed this strategy with the potential for creating comprehensive, tailored, damage-resistant, and ready-to-use supercapacitors.." (Page 5, line 15-22)

The innovation of the work is further emphasized in the Introduction: "Their rapid charge-discharge rates render them suitable for extreme environments, such as engine ignition systems that require high instantaneous power, demanding high working stability and damage resistance." (Page 2, line 13-16)

The key parameters of the PANI/C/SiOC-based supercapacitor are compared with those of recently reported 3D-printed PANI supercapacitors and rigid supercapacitors in Supplementary Table 1, to emphasize its distinctiveness and practical utility:

Supplementary Table 1. Comparison of the recently reported 3D-printed PANI supercapacitors and rigid supercapacitors.

Electrode (Structure)	Specific capacitance	Measurement	Mechanical performance	Damage resistance	Ref
PANI/Fe-Ni (Scaffold)	540.68 F/g (5 mV/s)	Two-electrode system	/	/	58
MnO_2/PANI (Interdigital structure)	575 F/g (0.4 A/g)	Asymmetric supercapacitor	/	/	59
PANI hydrogel (Printable)	422 F/g (0.2 A/g)	Three-electrode system	/	/	60
Graphene/ PANI (Mesh)	483.9 mF/cm^2 (0.5 mA/cm^2)	Symmetric supercapacitor	/	/	61
PANI/RGO (Interdigital structure)	1329 mF/cm^2 (5 mA/cm^2)	Symmetric supercapacitor	/	/	62
Porous carbon (Microlattice)	105 F/g	Three-electrode system	Compressive stress: ~10.45 MPa Modulus: 0.74 Gpa	/	63
$Cu(OH)_2$/Cu/Ceramic (Octet-truss lattice)	831 F/g (5 mA/cm^3)	Three-electrode system	Specific compressive stress: 30.02 MPa Specific energy absorption: 264.7 kJ/m^3	/	64
Ti_3C_2Tx-MXene/resin (Octet structure)	74 F/g (30 mV/s)	Three-electrode system	Compressive stress: ~12.5 MPa Modulus: 0.15 Gpa	/	65
(Ni, Co, Mn) Se/Carbon-rich lattices (Wave structure)	7.8 F/cm^2 (1 mA/cm^2)	Three-electrode system	Specific compressive stress: 9.52 MPa Specific modulus: 0.26 GPa Specific energy absorption: 18.33 kJ/m^3	Maintaining 60% capacitance after 5000 cycles under 3 MPa at 85 °C	66
Porous silicon (Plate)	20 Wh/kg	Symmetric supercapacitor	Tensile strength: 300 kPa Shear strength: 120 kPa	Maintaining 10 W h/kg under 300 kPa tensile stresses and 80 g vibratory accelerations	38
$NiCo_2O_4$/GF (Gyroid)	810 mF/cm^3	Asymmetric supercapacitor	Compressive stress: 1.4 MPa (GF substrate) Modulus: 12 MPa	/	67
PANI/C/SiOC (I-WP structure)	585.5 mF/cm^3 (3 mA/cm^3)	Symmetric supercapacitor	Compressive stress: 71.31 MPa Modulus: 2.72 GPa Energy absorption: 92.58 kJ/m3	Maintaining full functionality after impact (0.3 J/cm^3), under dynamic loading (0 to 18.83 MPa), and post electrolyte healing	This work

Detailed discussions of these comparison are included in the reivsed manuscript and the supplementary information: "Currently, efforts to develop 3D-printed PANI-based symmetric supercapacitors have gradually enriched the existing body of research (Supplementary Table 1). However, their performance under complex conditions has rarely been explored[58-62]. The PANI/C/SiOC electrode not only demonstrated comparable capacitance to the 3D-printed PANI-based symmetric supercapacitors but also excelled due to its ability to operate under harsh conditions. In comparison with other rigid supercapacitor electrodes or cells, the Cell I-WP showed enhanced compressive strength and energy absorption, managing more practical yet extreme conditions with high damage invulnerability[38,63-67]. Future modifications of the PANI/C/SiOC supercapacitor should aim to enhance temperature adaptability, such as frost and drying resistance, thereby extending its application to more severe environments." (Page 28, lines 8-18)

"Increasing research has focused on fabricating 3D-printed structuralized supercapacitors using PANI and its composites as active materials, attributed to their distinctive electrochemical and physical properties. These components can serve as self-standing electrodes for theoretical electrochemical tests using a three-electrode system or be integrated into symmetric supercapacitors for practical performance evaluation. However, the functionality of usable 3D-printed PANI-based supercapacitor cells, particularly under complex working conditions, such as loading or after damage, remains less explored. This study enhances the load-bearing capability and damage invulnerability of the 3D-printed PANI-based supercapacitor cell by employing a ceramic-based current collector and self-healable hydrogel to assemble the cell. The resulting cell demonstrated compressive stress, Young's modulus, and energy absorption of 70.61 MPa, 2.75 GPa, and 92.15 kJ/m^3, (Specific compressive stress: 197.23 MPa, specific modulus: 7.68 GPa, specific energy absorption: 257.4 kJ/m^3), while maintaining capacitance comparable to that of reported symmetric supercapacitors, promising to extend the potential applications of PANI-based supercapacitors. Compared to other rigid supercapacitors or electrodes, the mechanical performance of Cell I-WP exhibited advantages due to

the robust SiOC substrate. Furthermore, the cell's functionality was preserved under operational conditions post-impact (0.3 J/cm^3), under dynamic loading (0 to 18.83 MPa), and after electrolyte healing, scenarios not typically covered in currently reported studies but crucial for practical applications. Given the use of PVA hydrogel, future research should focus on enhancing the temperature adaptability of the cell, such as resistance to frost and drying, thereby broadening its utility in harsher environments." (Supplementary information, Pages 15-16)

2. The authors have presented the fabrication of several SiOC lattices with varying TPMS architects as electrodes and separators. Although they look pretty fancy, I cannot see the rationality of these structures and why they are chosen here. Of course, different structured lattices will show different mechanical response under impact. However, I think even without these structures, the SiOC ceramic itself is strong enough to provide extraordinary mechanical properties. If you think these structures can provide high surface area for electrolyte infilling, I will say the feature size (a few hundred microns) of printed structures is too large and increasing surface roughness/nanopores are better way to enlarge the accessible areas. Therefore, I think the relationship between these 3D structured electrodes and the devices mechanical/electrochemical performance is not clear. Besides, the separators are also printed into TPMS structures. I don't think such complex architectured separators are necessary. I know 3D printing is a hot area, but don't abuse the additively manufactured structural materials.

Response: Thank you very much for your professional and meticulous guidance. We will respond to each of your comments in detail.

(1) I cannot see the rationality of these structures and why they are chosen here

Response: Thanks! The concerns are justified rightly due to the scarcity of studies in this field, which has motivated our investigations. Accordingly, we designed various TPMS structures to assess their impact on redox processes, mechanical behaviour, active material loading, and electrochemical performance. Since TPMS structures are periodic, featuring repeating units. We have unified the unit

sizes of each TPMS electrode at 2 mm and the resolution (wall thickness) at 200 μm. Therefore, parameters such as surface area, porosity, and density are exclusively influenced by the TPMS structure category. Thus, the influence of the TPMS structure category can be studied. In response to your comments, illustrations have been included to further clarify the design rationale:

"The unit size of each TPMS electrode was unified to 2 mm with a resolution of 200 μm. Consequently, variations in parameters such as surface area, porosity, and density of the TPMS structures are solely attributable to the structure's category due to their inherent periodicity. This standardization allows for a systematic evaluation of how TPMS structures impact the electrochemical and mechanical performance of the electrodes and the supercapacitor cells." (Page 7, lines 15-21)

The resulting regulations are also enhanced to demonstrate the influence of TPMS structure category on mechanical and electrical performance:

"Cyclic voltammetry (CV) analysis, conducted at a scan rate of 10 mV/s, revealed that electrodes with solid plate structure and varying TPMS structures exhibited similar redox peaks (Fig. 3a)." (Pages 14, lines 10-12)

"Furthermore, the CV curves of the C/SiOC current collector exhibited no redox peaks, indicating that the pseudocapacitive reactions occurred mainly on the PANI active layer (Supplementary Fig. 4). Meanwhile, the consistency of the redox processes in electrodes with different TMPS structures demonstrated little influence from geometries on electrochemical behavior." (Page 14, lines 16-20)

"However, the electrodes with D and I-WP structures exhibited more pronounced charging and discharging plateaus, attributable to more efficient redox processes. Despite each electrode operating at the same volumetric charging and discharging current density, variations in active material loading (stemming from differences in the specific surface areas of each electrode) resulted in differing area-specific charging and discharging current densities. Consequently, the G and P structured electrodes

were operated at higher area-specific current densities, leading to less effective engagement of PANI in the redox processes due to inadequate faradaic redox kinetics. Therefore, it can be concluded that while all electrodes can operate at high current densities, those with a higher specific surface area can develop a larger active layer, thereby facilitating more sufficient redox processes and maximizing the electrochemical performance of the active layer. Specific capacitances for the G, D, P, and I-WP structured electrodes were calculated at 516.99, 601.06, 369.45, and 585.51 mF/cm^3, respectively, indicating an enhancement when compared to the PANI/C/SiOC electrode (91.77 mF/cm^3) and the solid plate structured C/SiOC current collector (13.95 mF/cm^3, Supplementary Fig. 4). While the TPMS structures do not significantly impact the electrochemical reactions themselves, they do affect specific capacitance by altering surface area availability and the amount of active material loading." (Page 16, lines 4-22)

"The SiOC substrate with G, D, P, and I-WP structures exhibited compressive strength of 26.63 ± 1.19, 72.39 ± 2.53, 13.94 ± 0.95, and 75.85 ± 2.04 MPa, respectively, and corresponding Young's modulus of 1.34 ± 0.09, 2.81 ± 0.12, 1.10 ± 0.06, and 2.71 ± 0.11 GPa (Fig. 4i)." (Page 22, lines 15-18)

"Additionally, the specific compressive stress (SCE) and specific modulus (SM) of the C/SiOC current collectors were calculated to assess the structural reinforcement capabilities of various TPMS structures (Supplementary Fig. 11a). The C/SiOC current collectors featuring G, D, P, and I-WP configurations registered SCE of 99.96 ± 4.43, 208.41 ± 7.26, 70.96 ± 4.76, and 212.42 ± 5.71 MPa, respectively. Notably, the I-WP structured C/SiOC demonstrated the highest specific compressive stress, indicating superior structural reinforcement compared to other designs with the same cell size and resolution." (Page 23, lines 5-12)

"Simulations revealed a homogeneous strain distribution in TPMS structures, with the D and I-WP structures exhibiting a more uniform stress distribution, mitigating localized stress concentrations (Fig.

4k). This uniformity also ensured continuous connectivity between C/SiOC and PANI, preventing separation." (Page 24, lines 4-8)

(2) I think even without these structures, the SiOC ceramic itself is strong enough to provide extraordinary mechanical properties.

Response: Thanks! While SiOC ceramics inherently possess strong theoretical mechanical properties, they require to be shaped into specific forms such as blocks, rods, or plates for practical applications. For instance, the work by Westover that you referenced in comment 1 utilized silicon shaped into plates. The material needs to be manufactured with appropriate thickness to fully leverage its performance but may lead to increased electrode weight. Thus, the structures employed in our research are designed not only to focus on mechanical properties but also to create hollow TPMS structures within the SiOC ceramic electrodes. This approach aims to improve space utilization and reduce weight while still maintaining adequate mechanical performance. Based on your comments, we have added some illustrations: "Since electrodes are typically engineered into specific configurations and dimensions to fully utilize their electrochemical and mechanical performance in device assemblies, a further significant advantage of SiOC substrates is their compatibility with 3D printing techniques for flexible configuration design. This adaptability facilitates the optimal use of confined spaces by electrode architecture adjustment, maximizing active material load and minimizing weight, thereby reducing energy self-consumption, while fine-tuning the mechanical properties[23-25]." (Page 3, lines 13-20)

Additionally, solid SiOC will not exhibit the expected satisfactory mechanical properties, primarily due to cracks and defects arising from the pyrolysis of polymeric precursors, which is a common issue for polymer-derived ceramics. This can be mitigated by incorporating hollow structures. Consequently, mechanical properties of solid SiOC have been included, and the necessity and advantages of creating TPMS structures are discussed:

"It is important to note that the creation of hollow structures within SiOC ceramics can effectively mitigate the formation of cracks and pores resulting from the pyrolysis of bulk polymeric precursors[18,20]. The compressive stress curve of solid SiOC indicated multiple peaks indicative of structural flaws and registered a compressive strength of 46.79 ± 5.6 MPa, with a higher standard deviation compared to those of TPMS-structured SiOC due to the defects (Supplementary Fig. 10). In contrast, the I-WP structured SiOC demonstrated a more uniform stress distribution with enhanced compressive strength, revealing that this configuration not only reduced weight and increased surface area, but also optimized mechanical behavior." (Pages 22-23)

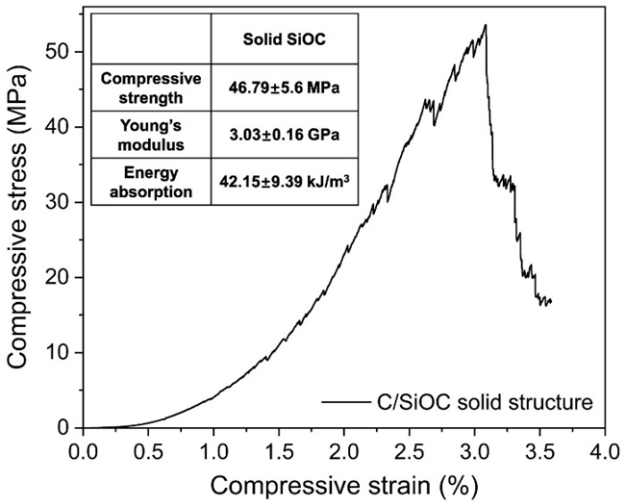

Supplementary Fig. 10 Compressive stress curve of solid SiOC.

"Supplementary Figure 10 displays the compressive stress curve of solid SiOC, which exhibits multiple peaks due to defects formed during pyrolysis, resulting in stress fluctuations. Consequently, solid SiOC did not demonstrate excellent mechanical behavior as expected. Its compressive strength, Young's modulus, and energy absorption measured 46.79 ± 5.6 MPa, 3.03 ± 0.16 GPa, and 42.15 ± 9.39 MPa, respectively. This is a typical issue for bulk polymer-derived ceramics (PDC), which can be mitigated by incorporating hollow structures within the PDC. Therefore, the creation of TPMS structures within SiOC proved to be an effective method to optimize its mechanical performance." (Supplementary information, Pages 9)

(3) I will say the feature size (a few hundred microns) of printed structures is too large and increasing surface roughness/nanopores are better way to enlarge the accessible areas.

Response: Thanks! The strategy of increasing surface roughness/nanopores to enlarge the accessible areas has been employed in this work through the use of PANI coating with nanorods arrayed morphology (Fig. 3d). Compared to the C/SiOC current collector (Fig. 2f), the coating enhances the roughness and introduces nanopores. To elucidate this aspect further, illustrations and a detailed description of the PANI nanorods' formation process have been added:

"Its facile formation of nanostructures on substrate materials contributed to an increase in surface roughness and the formation of nanopores, which collectively enlarged the accessible surface areas of the 3D electrodes." (Page 6, lines 14-17)

"The surface morphology of the PANI/C/SiOC electrodes, characterized by a porous structure with PANI nanorods arrayed homogeneously on the substrate (Fig. 3d), exhibited increased surface roughness and nanopores compared to the smooth C/SiOC current collector (Fig. 2f). This porous morphology led to enlarged accessible areas of the electrode, enhancing electrolyte penetration and ion transfer efficiency[44]. The nanorod morphology arose from the formation of amphiphilic aniline sulfate salt, which self-assembled into micelles in aqueous solution, serving as soft templates for the in-situ arraying of PANI nanorods on the C/SiOC surface[42]." (Page 17, lines 14-21)

(4) I think the relationship between these 3D structured electrodes and the devices mechanical/electrochemical performance is not clear.

Response: Thanks! The relationship between structures and performance is one of our research focal points, motivated by the scarcity of studies in this area, as illustrated in our response to comment (1). We have unified the unit sizes of each TPMS electrode at 2 mm and the resolution at 200 μm. Therefore,

parameters such as surface area, porosity, and density are exclusively influenced by the TPMS structure category. Under this premise, we have studied the impact of TPMS structure categories on mechanical and electrochemical performance. Relevant illustrations have been added to clarify this relationship, and the resulting regulations have been further refined:

"The unit size of each TPMS electrode was unified to 2 mm with a resolution of 200 μm. Consequently, variations in parameters such as surface area, porosity, and density of the TPMS structures are solely attributable to the structure's category due to their inherent periodicity. This standardization allows for a systematic evaluation of how TPMS structures impact the electrochemical and mechanical performance of the electrodes and the supercapacitor cells." (Page 7, lines 15-21)

The resulting regulations are also enhanced to demonstrate the influence of TPMS structure category on mechanical and electrical performance:

"Cyclic voltammetry (CV) analysis, conducted at a scan rate of 10 mV/s, revealed that electrodes with solid plate structure and varying TPMS structures exhibited similar redox peaks (Fig. 3a)." (Pages 14, lines 10-12)

"Furthermore, the CV curves of the C/SiOC current collector exhibited no redox peaks, indicating that the pseudocapacitive reactions occurred mainly on the PANI active layer (Supplementary Fig. 4). Meanwhile, the consistency of the redox processes in electrodes with different TMPS structures demonstrated little influence from geometries on electrochemical behavior." (Page 14, lines 16-20)

"However, the electrodes with D and I-WP structures exhibited more pronounced charging and discharging plateaus, attributable to more efficient redox processes. Despite each electrode operating at the same volumetric charging and discharging current density, variations in active material loading (stemming from differences in the specific surface areas of each electrode) resulted in differing area-specific charging and discharging current densities. Consequently, the G and P structured electrodes

were operated at higher area-specific current densities, leading to less effective engagement of PANI in the redox processes due to inadequate faradaic redox kinetics. Therefore, it can be concluded that while all electrodes can operate at high current densities, those with a higher specific surface area can develop a larger active layer, thereby facilitating more sufficient redox processes and maximizing the electrochemical performance of the active layer. Specific capacitances for the G, D, P, and I-WP structured electrodes were calculated at 516.99, 601.06, 369.45, and 585.51 mF/cm^3, respectively, indicating an enhancement when compared to the PANI/C/SiOC electrode (91.77 mF/cm^3) and the solid plate structured C/SiOC current collector (13.95 mF/cm^3, Supplementary Fig. 4). While the TPMS structures do not significantly impact the electrochemical reactions themselves, they do affect specific capacitance by altering surface area availability and the amount of active material loading." (Page 16, lines 4-22)

"The SiOC substrate with G, D, P, and I-WP structures exhibited compressive strength of 26.63 ± 1.19, 72.39 ± 2.53, 13.94 ± 0.95, and 75.85 ± 2.04 MPa, respectively, and corresponding Young's modulus of 1.34 ± 0.09, 2.81 ± 0.12, 1.10 ± 0.06, and 2.71 ± 0.11 GPa (Fig. 4i)." (Page 22, lines 15-18)

"Additionally, the specific compressive stress (SCE) and specific modulus (SM) of the C/SiOC current collectors were calculated to assess the structural reinforcement capabilities of various TPMS structures (Supplementary Fig. 11a). The C/SiOC current collectors featuring G, D, P, and I-WP configurations registered SCE of 99.96 ± 4.43, 208.41 ± 7.26, 70.96 ± 4.76, and 212.42 ± 5.71 MPa, respectively. Notably, the I-WP structured C/SiOC demonstrated the highest specific compressive stress, indicating superior structural reinforcement compared to other designs with the same cell size and resolution." (Page 23, lines 5-12)

"Simulations revealed a homogeneous strain distribution in TPMS structures, with the D and I-WP structures exhibiting a more uniform stress distribution, mitigating localized stress concentrations (Fig.

4k). This uniformity also ensured continuous connectivity between C/SiOC and PANI, preventing separation." (Page 24, lines 4-8)

(5) I don't think such complex architectured separators are necessary.

Response: Thanks! It is necessary that the strategy should maintain the same configuration between the electrode and separator, as both serve as load-bearing components in this work. These components should exhibit periodicity and coherence to uniformly distribute stress without introducing stress concentration points. Using separators that do not match the mechanical performance of the SiOC electrodes would create a weak point in the cell. Consequently, the mechanical performance threshold would then be determined by the weaker separators rather than the holistic load-bearing system, in line with the "cask effect theory". Additionally, employing a separator with different architectures would disrupt the mechanical periodicity and coherence, resulting in a loss of mechanical isotropy in the cell. These points have been further elaborated in the manuscript:

"Electrodes were fabricated via in-situ growth of active materials on the TPMS-structured SiOC, paired with an insulating SiOC separator that shared the same TPMS design. The hydrogel electrolyte was infused into the hollow spaces to complete a hydrogel-infused TPMS lattice configuration as a ready-to-use supercapacitor cell. Since this design was reinforced by the continuous SiOC skeleton, weak phases and anisotropic mechanical behavior common in lamellar or sandwich structures can be avoided. This uniform continuity and periodicity between the electrode and separator allowed the skeleton to distribute stress evenly, mitigating stress concentration." (Page 5, lines 11-19)

"Furthermore, the structural continuity and periodicity between the electrodes and separator contributed to a holistic reinforcement in the cell, resulting in isotropic mechanical behavior." (Page 10, lines 19-21)

(6) I know 3D printing is a hot area, but don't abuse the additively manufactured structural materials.

Response: We sincerely appreciate your critiques and instructions! We apologize if any "abuse" has occurred in this work. We will thoroughly reflect on our research to prevent any future instances of "abuse".

3D printing techniques have become one of the most promising methods for transforming materials studied theoretically into practical devices. These techniques are characterized by standardized procedures, programmable modifications, real-time process adjustments, rapid production, and minimal material waste, and are widely employed to manufacture functional devices, including supercapacitors. As theoretical research continues to yield a variety of active energy storage materials, their integration into practical applications necessitates appropriate media and strategic approaches. 3D printing of structural materials offers extensive flexibility in device design, enabling customized solutions tailored to specific application requirements, which improves adaptability and scalability. This adaptability extends to the design of assembly sockets in series and parallel configurations, and encapsulation using a standardized, process-driven approach, all facilitated by computer-aided manufacturing. Additionally, 3D printing's capability to integrate bespoke connectors and sockets enhances compatibility with various assembly methods, promising to simplify traditional processes that typically rely on complex circuits and wires. The ease of sharing digital structures could further promote the establishment of production standards and collaborative development. While this process is crucial, these processes often receive less attention compared to theoretical studies. Therefore, we utilized the 3D printing technology to explore fundamental processes and trying to develop a strategy for robust supercapacitor design.

We apologize once again if any "abuse" of 3D printing technology has occurred in this work. Additional discussion on the motivation for employing 3D printing technology has been included:

"Another advantage of 3D printing lies in its flexibility in cell architecture design. Although this work employed a conventional electrode shape to standardize the calculation and evaluation of theoretical

performance, the further design of seamless joints between electrodes and separators is straightforward and adaptable. The design of interlocking structures can offer a diverse assembly approach (as illustrated in Fig. 5i), enabling the creation of customized and stable devices tailored to various application requirements with firmer and more robust assembly manners." (Pages 28-29)

"Notably, the cell design can also incorporate connectors, enabling series or parallel configurations. The incorporation of bespoke connectors and sockets into the cells can accommodate various assembly methods, streamlining traditional splicing and assembly processes that typically involve complex circuits and wires. This versatility is instrumental in the assembly of expansive supercapacitor devices or modulating output voltages to cater to a spectrum of applications. Furthermore, this structurally strengthened strategy can be promoted to other supercapacitor material systems, since the active materials coated on the current collector and electrolyte solution swollen in the hydrogel are replaceable. Computer-aided manufacturing also supports real-time adjustments to processes and standardization of production. Furthermore, the ease of sharing digital structures could enhance the establishment of production standards and foster collaborative development[68]." (Pages 29-30)

"Since electrodes are typically engineered into specific configurations and dimensions to fully utilize their electrochemical and mechanical performance in device assemblies, a further significant advantage of SiOC substrates is their compatibility with 3D printing techniques for flexible configuration design. This adaptability facilitates the optimal use of confined spaces by electrode architecture adjustment, maximizing active material load and minimizing weight, thereby reducing energy self-consumption, while fine-tuning the mechanical properties[23-25]." (Page 3, line 12-19)

"Furthermore, the employment of scalable and customizable 3D printing techniques endows this strategy with the potential for creating comprehensive, tailored, damage-resistant, and ready-to-use supercapacitors." (Page 5, lines 19-22)

3. The authors fabricated four types of TPMS lattices, Gyroid, Diamond, Primitive, and I-WP with different porosity, relative density, and surface area. I think that direct comparison of these devices mechanical properties and electrochemical performance is unreasonable since so many structural parameters are different. We cannot simply conclude which structure is the best. Besides, for the lattice structures, the scale effect is very important. If you increase the printing resolution, scaling law in Ashby map will be significantly different. Current resolution is too big for stereolithography-based 3D printing.

Response: We appreciate the reviewer for the comments! The first concern aligns with comments 2.1 and 2.4 regarding the design concept of the TPMS structures. The four TPMS structures were derived from distinct mathematical expressions. By unifying their unit sizes and resolutions, parameters such as porosity, relative density, and surface area vary solely according to the TPMS structure category. Based on this unification, the influence of TPMS structure categories on mechanical and electrochemical performance can be compared. To clarify the design objectives, illustrations have been enhanced:

"The unit size of each TPMS electrode was unified to 2 mm with a resolution of 200 μm. Consequently, variations in parameters such as surface area, porosity, and density of the TPMS structures are solely attributable to the structure's category due to their inherent periodicity. This standardization allows for a systematic evaluation of how TPMS structures impact the electrochemical and mechanical performance of the electrodes and the supercapacitor cells." (Page 7, lines 15-21)

The resulting regulations are also enhanced to demonstrate the influence of TPMS structure category on mechanical and electrical performance:

"Cyclic voltammetry (CV) analysis, conducted at a scan rate of 10 mV/s, revealed that electrodes with solid plate structure and varying TPMS structures exhibited similar redox peaks (Fig. 3a)." (Pages 14, lines 10-12)

"Furthermore, the CV curves of the C/SiOC current collector exhibited no redox peaks, indicating that the pseudocapacitive reactions occurred mainly on the PANI active layer (Supplementary Fig. 4). Meanwhile, the consistency of the redox processes in electrodes with different TMPS structures demonstrated little influence from geometries on electrochemical behavior." (Page 14, lines 15-19)

"However, the electrodes with D and I-WP structures exhibited more pronounced charging and discharging plateaus, attributable to more efficient redox processes. Despite each electrode operating at the same volumetric charging and discharging current density, variations in active material loading (stemming from differences in the specific surface areas of each electrode) resulted in differing area-specific charging and discharging current densities. Consequently, the G and P structured electrodes were operated at higher area-specific current densities, leading to less effective engagement of PANI in the redox processes due to inadequate faradaic redox kinetics. Therefore, it can be concluded that while all electrodes can operate at high current densities, those with a higher specific surface area can develop a larger active layer, thereby facilitating more sufficient redox processes and maximizing the electrochemical performance of the active layer. Specific capacitances for the G, D, P, and I-WP structured electrodes were calculated at 516.99, 601.06, 369.45, and 585.51 mF/cm^3, respectively, indicating an enhancement when compared to the PANI/C/SiOC electrode (91.77 mF/cm^3) and the solid plate structured C/SiOC current collector (13.95 mF/cm^3, Supplementary Fig. 4). While the TPMS structures do not significantly impact the electrochemical reactions themselves, they do affect specific capacitance by altering surface area availability and the amount of active material loading." (Page 16, lines 4-22)

"The SiOC substrate with G, D, P, and I-WP structures exhibited compressive strength of 26.63 ± 1.19, 72.39 ± 2.53, 13.94 ± 0.95, and 75.85 ± 2.04 MPa, respectively, and corresponding Young's modulus of 1.34 ± 0.09, 2.81 ± 0.12, 1.10 ± 0.06, and 2.71 ± 0.11 GPa (Fig. 4i)." (Page 22, lines 15-18)

"Additionally, the specific compressive stress (SCE) and specific modulus (SM) of the C/SiOC current collectors were calculated to assess the structural reinforcement capabilities of various TPMS structures (Supplementary Fig. 11a). The C/SiOC current collectors featuring G, D, P, and I-WP configurations registered SCE of 99.96 ± 4.43, 208.41 ± 7.26, 70.96 ± 4.76, and 212.42 ± 5.71 MPa, respectively. Notably, the I-WP structured C/SiOC demonstrated the highest specific compressive stress, indicating superior structural reinforcement compared to other designs with the same cell size and resolution." (Page 23, lines 5-12)

"Simulations revealed a homogeneous strain distribution in TPMS structures, with the D and I-WP structures exhibiting a more uniform stress distribution, mitigating localized stress concentrations (Fig. 4k). This uniformity also ensured continuous connectivity between C/SiOC and PANI, preventing separation." (Page 24, lines 4-9)

Additionally, this study aims to investigate how TPMS structures influence performance using existing printing technologies. Advancing printing technology to breakthrough the physical limitation is not the primary focus of this work. The current resolution of 200 μm is suitably fine for vat-polymerization 3D printing for the regulation study, particularly for ceramic structures, which typically range from several hundred micrometers to centimeters in resolution. Meanwhile, this study utilizes DLP (Digital Light Processing) 3D printing rather than stereolithography-based 3D printing, though both techniques rely on UV-curing of feedstock that are similar. However, they differ in their light sources and printing approaches: while stereolithography uses a single laser beam to cure feedstock in 2D layers following a point-line-surface path, DLP employs a UV projector to cure entire layers simultaneously, enhancing printing efficiency. Conversely, stereolithography offers superior printing accuracy. Therefore, each technique has distinct application targets. Based on the comments, further illustrations of the fabrication process and 3D printing techniques have been added: "Utilizing the precision and high efficiency of vat photopolymerization, rapid and accurate formations can be achieved using a digital light processing (DLP) printer[42,43]." (Page 6, lines 6-8)

"Specifically, triply periodic minimal surface (TPMS) substrates were fabricated using a digital light processing (DLP) printer (Max UV385, Asiga) equipped with a 385 nm UV light source. The substrates were created from a photocurable-modified methyl-silsesquioxane resin (SILRES MK, Wacker-Chemie). During the printing process, exposure time of each layer was maintained at 2 seconds, current intensity was set at 15 mW/cm^3, and the layer thickness was 50 μm." (Page 31, lines 1-7)

4. The advantage of supercapacitors is their high-power density, but their low energy density is always a problem that has hampered the real application. The authors used ceramic as electrode scaffolds that not only introduce complex post-processing procedures (conductive carbon and PANI coating), but also increase the dead weight to decrease the gravimetric energy density. This strategy cannot reconcile the mechanical strength and energy density. Besides, I'm not sure if SiO contributes any electrochemical capacitance. Please provide XPS analysis of Si before and after stability tests.

Response: We extend our gratitude for your constructive comments! The process that employing 3D printing simplifies rather than complicates the post-processing procedures if the entire device production process is considered. Measuring the theoretical performance of supercapacitor materials by applying active materials onto a commercial current collector is straightforward, yet it is insufficient for practical applications. To assemble a functional supercapacitor, components such as separators, current collectors, wires, joints, and shields must all be considered, and coating, assembly, and encapsulation procedures are still required. The fabrication of these consumables involves complex post-processing procedures, we cannot ignore these complexities just because they were purchased from suppliers. However, 3D printing promises to streamline these post-processing steps by integrating joints, current collectors, and separators into a single usable current collector, achieving integrated or modular and standardized production, unlike the use of commercial consumables from different suppliers with varying production standards. The prospect of realizing all printed energy storage devices on a single production line is promising by advancements in 3D printing technology.

Additional discussion has been added to clarify these processes: "Notably, the cell design can also incorporate connectors, enabling series or parallel configurations. The incorporation of bespoke connectors and sockets into the cells can accommodate various assembly methods, streamlining traditional splicing and assembly processes that typically involve complex circuits and wires. This versatility is instrumental in the assembly of expansive supercapacitor devices or modulating output voltages to cater to a spectrum of applications. Furthermore, this structurally strengthened strategy can be promoted to other supercapacitor material systems, since the active materials coated on the current collector and electrolyte solution swollen in the hydrogel are replaceable. Computer-aided manufacturing also supports real-time adjustments to processes and standardization of production. Furthermore, the ease of sharing digital structures could enhance the establishment of production standards and foster collaborative development[68]." (Pages 29-30)

Additionally, C/SiOC-based electrodes will not increase the dead weight, owing to their lightweight properties. For comparison, consider a commonly used Ni current collector, which has a density of 8.99 g/cm^3. In contrast, the densities of C/SiOC range from 2.5 to 2.76 g/cm^3, indicating a substantial reduction in weight that will enhance the gravimetric energy density of the devices. In response to the comment, we have expanded the relevant discussion in the manuscript: "Additionally, the densities of G, D, P, and I-WP structured C/SiOC were recorded at 0.73, 0.92, 0.99, and 0.50 g/cm^3, respectively. Consequently, their material densities (structure density/entity rate) were calculated to be 2.72, 2.64, 2.76, and 2.5 g/cm^3, respectively, varied due to the different surface area and coating contents. The maximum value of 2.76 g/cm^3 still indicated a significant weight reduction when compared to traditional Ni-based (8.99 g/cm^3) porous current collectors, thereby underscoring its superiority in enhancing the gravimetric energy density of the assembled devices." (Pages 13-14)

To demonstrate the electrochemical inertness of C/SiOC, its electrochemical performance was investigated. Since the XRD and XPS analyses of the electrode before stability testing have been included, the corresponding analyses after stability testing have also been added.:

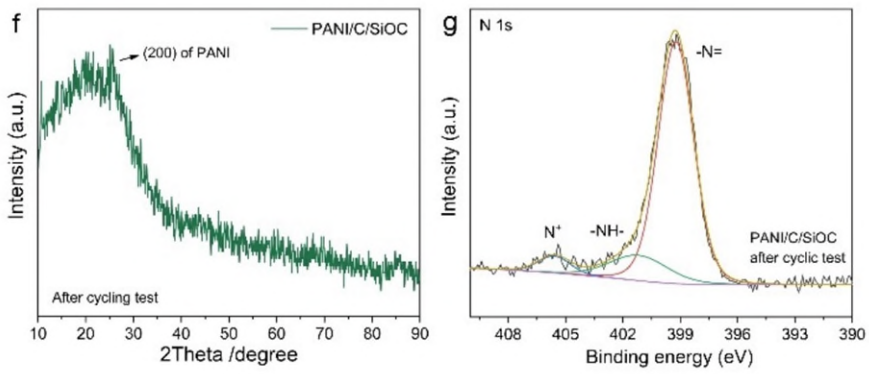

Fig. 5 Self-healing performance of PVA hedrogel and scalability of the cells: (e) Cycling stability of self-healed Cell I-WP; (f) XRD pattern and (g) XPS C 1s deconvoluted peaks of PANI/C/SiOC after cycling test

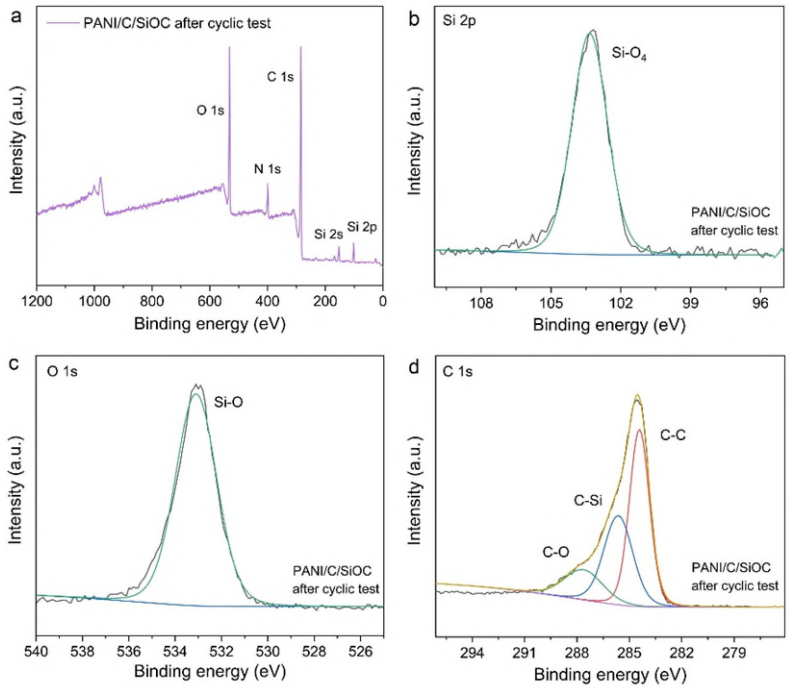

Supplementary Fig. 15 (a) XPS survey spectra of PANI/C/SiOC after cyclic test. XPS deconvoluted peaks of (b) Si 2p, (c) O 1s, and (d) C 1s of PANI/C/SiOC after cyclic test.

Detailed discussions of these characterization are included in the reivsed manuscript and the supplementary information: "The XRD pattern of the PANI/C/SiOC electrode after cycling tests consistently exhibited the peak at 25.6°, which corresponded to the (200) crystal planes of PANI. (Fig. 5f). Concurrently, XPS analysis indicated minimal changes in the atomic states, except that the high-

resolution N 1s spectra showed a decrease in the intensity of the benzenoid amine -NH-, attributed to the formation of pernigraniline base following complete discharge. Furthermore, high-resolution Si 2p spectra revealed no significant alterations from its initial state, suggesting that the C/SiOC current collector did not participate in the pseudocapacitive reaction (Fig. 5f and Supplementary Fig. 15)." (Page 27, lines 8-15)

"XPS spectroscopy was employed to analyze the atomic states of elements on the surfaces of PANI/C/SiOC electrodes after cyclic testing (Supplementary Fig. 15). Peaks corresponding to Si 2s, Si 2p, O 1s, and C 1s were still identified in the survey spectra, indicating the preservation of the electrode's composition after prolonged cycling. High-resolution N 1s spectra revealed a reduction in the intensity of the benzenoid amine -NH-, which was attributed to the formation of pernigraniline base after complete discharge (Fig. 5g). The Si 2p and O 1s spectra displayed deconvoluted peaks assigned to Si-O_4 and Si-O, respectively, while the deconvoluted C 1s peak identified C-O, C-Si, and C-C bonds. These findings suggest minimal changes compared to the initial PANI/C/SiOC electrode and confirm that the C/SiOC current collector did not engage in the pseudocapacitive reaction." (Supplementary information, Pages 13-14)

The electrochemical performance of supercapacitors using C/SiOC electrodes was further tested and compared with that of TPMS structured electrodes to demonstrate that C/SiOC does not contribute to pseudocapacitance:

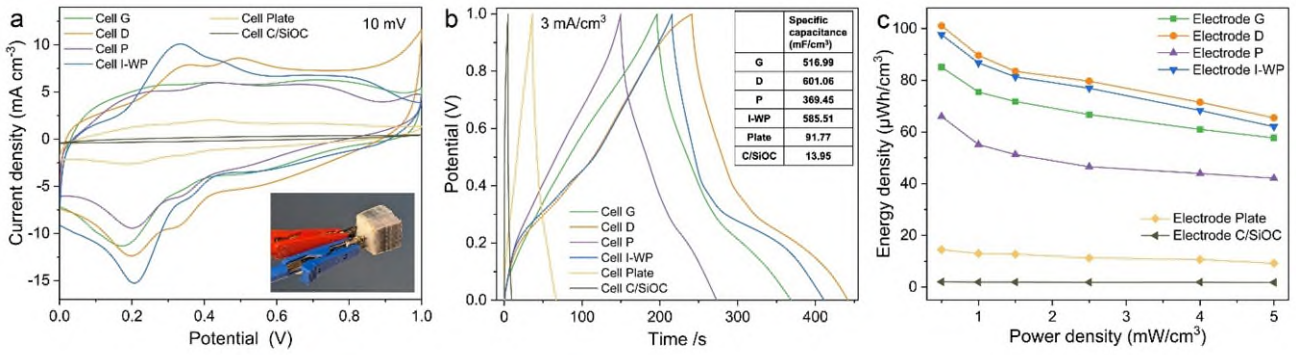

Fig. 3 Electrochemical properties and characterization of PANI/C/SiOC cells: Electrochemical properties of cell with different electrode structures: (a) CV curves, (b) GCD curves, and (c) Ragone plots (power density vs energy density)

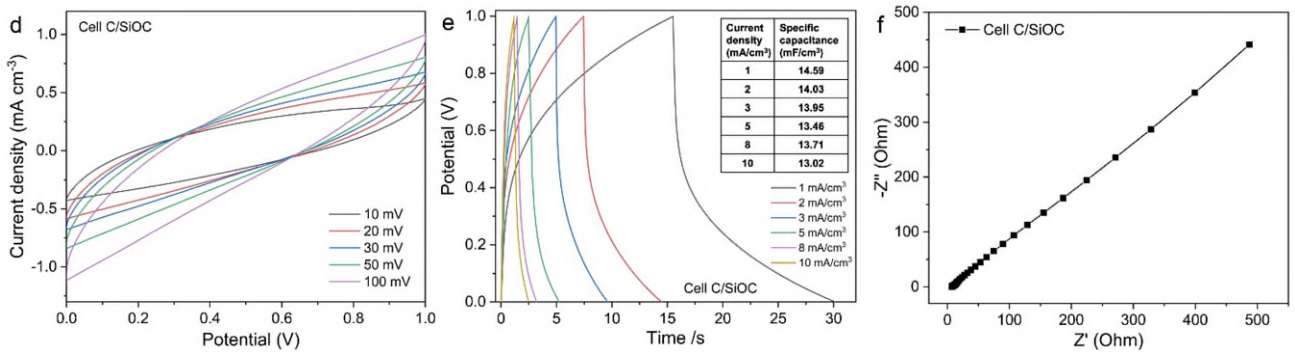

Supplementary Fig. 4 Electrochemical performance of Cell with PANI/C/SiOC and C/SiOC plates as electrodes: (d) CV curves, (e) GCD curves, and (f) EIS plots of Cell C/SiOC.

Detailed discussions of these comparison are included in the reivsed manuscript and the supplementary information: "Cyclic voltammetry (CV) analysis, conducted at a scan rate of 10 mV/s, revealed that electrodes with solid plate structure and varying TPMS structures exhibited similar redox peaks (Fig. 3a)." "Furthermore, the CV curves of the C/SiOC current collector exhibited no redox peaks, indicating that the pseudocapacitive reactions occurred mainly on the PANI active layer (Supplementary Fig. 4)." (Page 14, lines 10-20)

"Conversely, the CV curves of the Cell C/SiOC showed no redox peaks, confirming that the pseudocapacitive reactions scarcely involve the C/SiOC current collector. Nonetheless, the Cell C/SiOC still exhibited little energy storage capacity with a specific capacitance of approximately 14 mF/cm^3 at different current density, primarily due to its electric double-layer capacitance characteristics, which minimally contribute to the overall capacitance of the TMPS structured cells." (Supplementary information, Pages 4, lines 9-15)

5. I also noticed that the integrated electrode, separator, and PVA hydrogel electrolyte are assembled into a FDM printed mold, as shown in Fig. 2a. That means you put an ultra-strong system into a weak container. Have you considered the whole system as a whole? Unless you make an impact resistant case, otherwise all works discussed in this paper are meaningless.

Response: We appreciate the reviewer for the comments! In this work, FDM-printed molds were only utilized for cell assembly. After hydrogel formation, the cells were detached from the molds, and no containers or cases were employed during performance measurements, as detailed in the original manuscript. To enhance clarity, conspicuous illustrations have been included in the schematic diagram (Fig. 2a), and additional explanations have been provided in the main text:

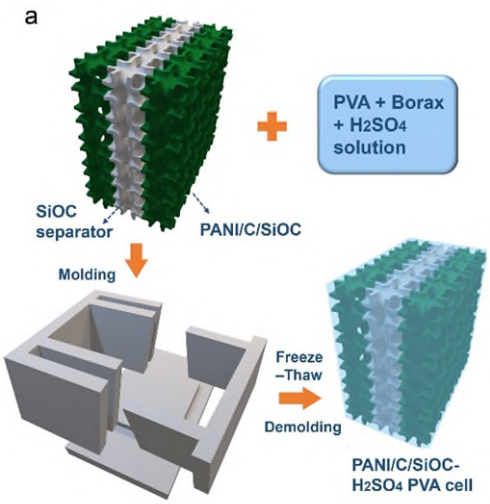

Fig. 2 (a) Diagram of the assembly process

"Upon demolding, self-standing and independently functioning supercapacitor cells were produced." (Page 7, lines 2-3)

"Post-integration, the assembled cells were detached from the molds". (Page 9, lines 7-8)

"Besides, the detachable mold, with dimensions meticulously matched to the cell, allows for complete and nondestructive extraction after the assembly." (Page 11, lines 18-20)

6. In comparison, the flexible supercapacitor is a better solution to achieve high impact tolerance and excellent electrochemical performance by combining flexible electrodes and gel electrolytes. (e.g., Yang, Yongrui, et al. "Recent progress in the all-solid-state flexible supercapacitors." SmartMat 3.3 (2022): 349-383.)

Response: We appreciate the reviewer for the comments! Flexible supercapacitors represent a compelling solution to achieve high impact tolerance and excellent electrochemical performance by combining flexible electrodes and gel electrolytes. They are poised to play a decisive role in the field of energy storage devices. In the revised manuscript, the significance of this research area has been highlighted in the introduction, and recommended references have been incorporated: "Flexible supercapacitors employing hydrogel electrolytes, as demonstrated in Yang's research[35-37], exhibit considerable potential for use under complex load-bearing conditions, distinguished by their high impact tolerance and superior electrochemical performance." (Page 4, lines 10-13)

The recommended references have been added to support the point:

35. Yang, Y. et al. Recent Progress in the All-Solid-State Flexible Supercapacitors. *SmartMat.* **3**, 349-383 (2022).

36. Yang, Y. et al. Solid-State Double-Network Hydrogel Redox Electrolytes for HighPerformance Flexible Supercapacitors. *ACS Appl. Mater. Interfaces* **13**, 34168-34177 (2021).

37. Yang, Y. et al. All-Solid-State Asymmetric Supercapacitors with Novel Ionic Liquid Gel Electrolytes. *ACS Appl. Mater. Interfaces* **2**, 3906-3914 (2020).

38. S. Westover, A. et al. A Multifunctional Load-Bearing Solid-State Supercapacitor. *Nano Lett.* **14**, 3197-3202 (2014).

Although flexible supercapacitors demonstrate excellent electrochemical and mechanical performance, certain applications may still necessitate the use of rigid supercapacitors. Consequently, this work could offer insights or serve as a reference. We sincerely hope that while the field of flexible

supercapacitors continues to thrive, our contributions will address some of the existing research gaps in the area of rigid supercapacitors. To this end, we have added discussions to underscore the potential and requirement for rigid supercapacitors: "Meanwhile, rigid and impact-resistant supercapacitors are also essential in specific applications such as aerospace, underwater equipment, and new energy vehicles[38]. Consequently, enhancing hydrogel supercapacitors with 3D-printed SiOC lattice-based electrodes holds promise for broadening their application scope." (Page 4, lines 14-18)

Reviewer #2

The manuscript (Manuscript Number: NCOMMS-24-13148, Title: Impact-Resistant Supercapacitor by Hydrogel-Infused Lattice) reports Impact-resistant and ready-to-use supercapacitors constructed from self-healable hydrogel electrolytes infused structurally reinforced lattice electrodes. Moreover, 3D-printed conductive C/SiOC current collectors provided superior mechanical protection. The designs and fabrication of the flexible supercapacitors are interesting. I will suggest the publication of the works after minor revision. Here are some questions:

1. Will the electrochemical performance of the supercapacitor attenuate after repeated twist and stretch.

Response: Thank you very much for your professional and meticulous guidance! The supercapacitor was reinforced using rigid and periodic SiOC-based electrodes. Unlike flexible supercapacitors, they cannot undergo substantial twisting and stretching, but they can withstand slight deformations at the interfaces between electrodes and separators (Supplementary Figures 14c and f), which is also this supercapacitor's vulnerable points. Initially, we focused on evaluating electrochemical stability after self-repair of these vulnerable points, potentially overlooking more practical conditions of repeated twists and stretches. Thank you once again for your insightful feedback. We have now assessed the electrochemical performance of the supercapacitor under repeated twists and stretching at these critical interfaces, further demonstrating its resistance to damage under practical conditions:

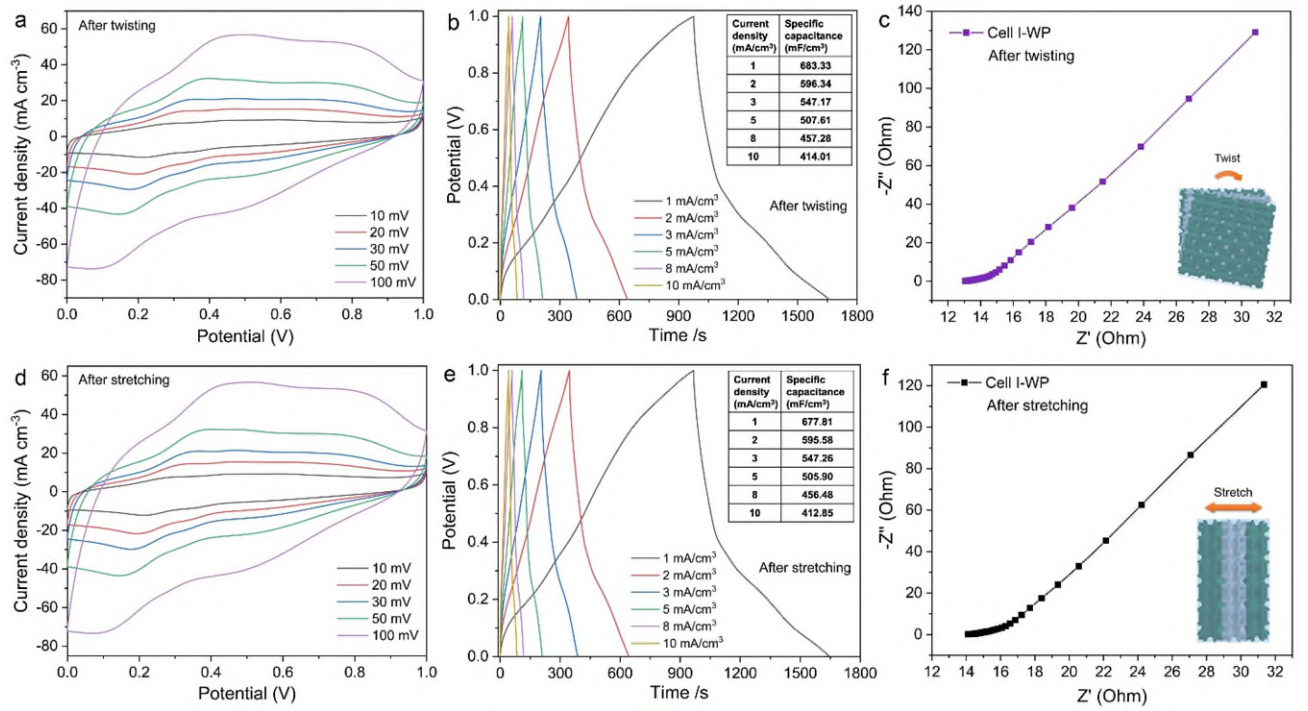

Supplementary Fig. 14 Electrochemical performance of Cell I-WP after twisting and stretching. (a) CV curves, (b) GCD curves, and (c) EIS plots of Cell I-WP after twisting 100 times. (d) CV curves, (e) GCD curves, and (f) EIS plots of Cell I-WP after stretching 100 times.

Detailed discussions of these evaluations are included in the reivsed manuscript and the supplementary information: "It also ensured high working stability under more complex and practical conditions. Electrochemical behavior and capacitance of Cell I-WP remained largely unchanged after 100 cycles of twisting and stretching at the interfaces between electrodes and separators, respectively, demonstrating significant adaptability to damaging environmental conditions (Supplementary Fig. 14)." (Page 25, lines 13-17)

"To assess the working stability of the Cell I-WP under damaging yet practical conditions, its electrochemical performance was evaluated after 100 cycles of twisting followed by 100 cycles of stretching, respectively (Supplementary Fig. 14). The CV curves (10-100 mV/s) maintained normal electrochemical behavior compared to the initial cell. Both GCD curves (1-10 mA/cm^3) and EIS spectra (0.01 Hz to 100 kHz) exhibited similar shapes. The specific capacitance of the Cell I-WP, after

cyclic twisting and stretching, was measured at 547.17 mF/cm^3 and 547.26 mF/cm^3 at current densities of 3 mA/cm^3, respectively, demonstrating little difference from the initial Cell." (Supplementary information, Page 13)

2. On Page 23, The authors wrote: "Upon recontact, these cleaved bonds underwent reformation, facilitating the regeneration and self-repair of the crosslinked network (Fig. 3g and 5e)", please check the name of the Figure 3 (g) carefully.

Response: We highly appreciate the reviewer for pointing this out! We apologize for the error in the original manuscript where the labels for Figs. 3g and 3e were reversed. This has been corrected in the revised manuscript:

"Fig. 3 (f) XPS deconvoluted peaks of N 1s for PANI/C/SiOC; (g) FT-IR spectrum of freeze-dried PVA" (Page 15, lines 12-13)

3. The authors wrote: "The XRD pattern of PANI/C/SiOC displayed a small but sharp peak at 25.6°, corresponding to the (200) crystal planes of emeraldine salt (Fig. 1c)", but it is (220) crystal planes into Fig. 1c, Which one is correct.

Response: Thank you very much for your careful review of the manuscript! The peak at 25.6° in the XRD pattern should be assigned to the (200) crystal planes of emeraldine salt. We apologize for the error and have corrected Fig. 1c in the revised manuscript. Additionally, we have included references to support this conclusion:

"The XRD pattern of PANI/C/SiOC displayed a small but sharp peak at 25.6°, corresponding to the (200) crystal planes of emeraldine salt (Fig. 1c) [32,44]." (Page 8, lines 21-22)

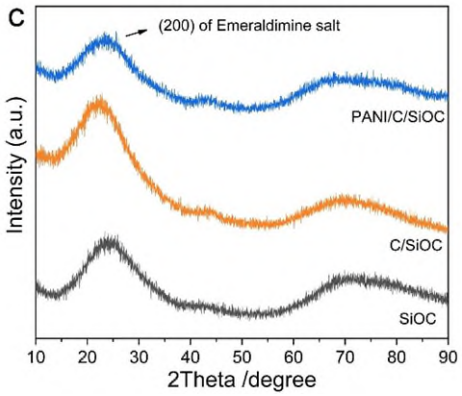

Fig. 1 (c) XRD patterns of the SiOC, C/SiOC, and PANI/C/SiOC

4. The samples should be characterized by spectroscopic techniques after long cycling tests. The cycling stability experiments need to be performed again minimum for 5000 cycles.

Response: We are grateful for your valuable suggestion. In the revised manuscript, the cycling stability experiment was repeated for 5,000 cycles. Afterward, the electrodes were removed from the supercapacitor for spectroscopic characterization to evaluate their functional integrity:

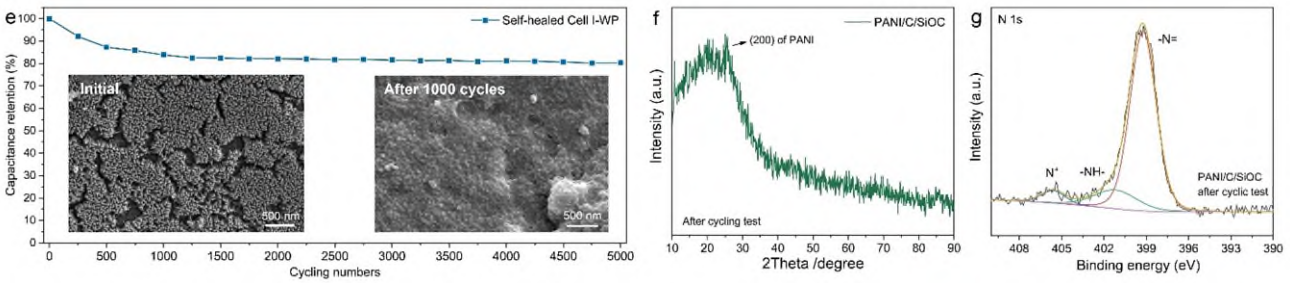

Fig. 5 Self-healing performance of PVA hedrogel and scalability of the cells: (e) Cycling stability of self-healed Cell I-WP; (f) XRD pattern and (g) XPS C 1s deconvoluted peaks of PANI/C/SiOC after cycling test

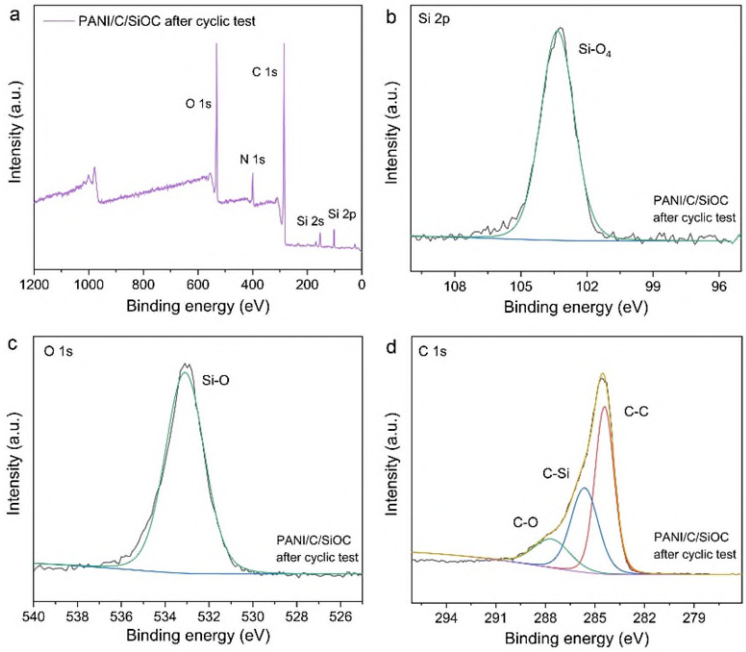

Supplementary Fig. 15 (a) XPS survey spectra of PANI/C/SiOC after cyclic test. XPS deconvoluted peaks of (b) Si 2p, (c) O 1s, and (d) C 1s of PANI/C/SiOC after cyclic test.

Detailed discussions of these characterization are included in the reivsed manuscript and the supplementary information: "Accordingly, we assessed its cyclic durability for 5000 cycles at a current density of 10 mA/cm^3. The cell demonstrated a rapid capacitance attenuation to 83.86% of its initial value after 1000 cycles, while remaining relatively stable during the rest cycles that maintained 80.31% capacitance, reflecting an acceptable level of cyclic stability and reliability of the repaired PVA hydrogel electrolyte (Fig. 5e)." (Pages 26-27)

"The XRD pattern of the PANI/C/SiOC electrode after cycling tests consistently exhibited the peak at 25.6°, which corresponded to the (200) crystal planes of PANI. (Fig. 5f). Concurrently, XPS analysis indicated minimal changes in the atomic states, except that the high-resolution N 1s spectra showed a decrease in the intensity of the benzenoid amine -NH-, attributed to the formation of pernigraniline base following complete discharge. Furthermore, high-resolution Si 2p spectra revealed no significant alterations from its initial state, suggesting that the C/SiOC current collector did not participate in the pseudocapacitive reaction (Fig. 5f and Supplementary Fig. 15)." (Page 27, lines 8-15)

"XPS spectroscopy was employed to analyze the atomic states of elements on the surfaces of PANI/C/SiOC electrodes after cyclic testing (Supplementary Fig. 15). Peaks corresponding to N 1s Si 2s, Si 2p, O 1s, and C 1s were still identified in the survey spectra, indicating the preservation of the electrode's composition after prolonged cycling. High-resolution N 1s spectra revealed a reduction in the intensity of the benzenoid amine -NH-, which was attributed to the formation of pernigraniline base after complete discharge (Fig. 5g). The Si 2p and O 1s spectra displayed deconvoluted peaks assigned to $Si-O_4$ and Si-O, respectively, while the deconvoluted C 1s peak identified C-O, C-Si, and C-C bonds. These findings suggested minimal changes compared to the initial PANI/C/SiOC electrode and confirmed that the C/SiOC current collector did not engage in the pseudocapacitive reaction." (Supplementary information, Pages 13-14)

5. Can authors compare the key material parameters of PANI/C/SiOC prepared in this work with the prior-art and other available materials for supercapacitor application?

Response: We sincerely appreciate your constructive comments. The key parameters of the PANI/C/SiOC-based supercapacitor are compared with those of recently reported 3D-printed PANI supercapacitors and rigid supercapacitors in Supplementary Table 1, to emphasize its distinctiveness and practical utility:

Supplementary Table 1. Comparison of the recently reported 3D-printed PANI supercapacitors and rigid supercapacitors.

Electrode (Structure)	Specific capacitance	Measurement	Mechanical performance	Damage resistance	Ref
PANI/Fe-Ni (Scaffold)	540.68 F/g (5 mV/s)	Two-electrode system	/	/	58
MnO_2/PANI (Interdigital structure)	575 F/g (0.4 A/g)	Asymmetric supercapacitor	/	/	59
PANI hydrogel (Printable)	422 F/g (0.2 A/g)	Three-electrode system	/	/	60
Graphene/ PANI (Mesh)	483.9 mF/cm^2 (0.5 mA/cm^2)	Symmetric supercapacitor	/	/	61
PANI/RGO (Interdigital structure)	1329 mF/cm^2 (5 mA/cm^2)	Symmetric supercapacitor	/	/	62
Porous carbon (Microlattice)	105 F/g	Three-electrode system	Compressive stress: ~10.45 MPa Modulus: 0.74 Gpa	/	63
$Cu(OH)_2$/Cu/Ceramic (Octet-truss lattice)	831 F/g (5 mA/cm^3)	Three-electrode system	Specific compressive stress: 30.02 MPa Specific energy absorption: 264.7 kJ/m^3	/	64
Ti_3C_2Tx-MXene/resin (Octet structure)	74 F/g (30 mV/s)	Three-electrode system	Compressive stress: ~12.5 MPa Modulus: 0.15 Gpa	/	65
(Ni, Co, Mn) Se/Carbon-rich lattices (Wave structure)	7.8 F/cm^2 (1 mA/cm^2)	Three-electrode system	Specific compressive stress: 9.52 MPa Specific modulus: 0.26 GPa Specific energy absorption: 18.33 kJ/m^3	Maintaining 60% capacitance after 5000 cycles under 3 MPa at 85 °C	66
Porous silicon (Plate)	20 Wh/kg	Symmetric supercapacitor	Tensile strength: 300 kPa Shear strength: 120 kPa	Maintaining 10 W h/kg under 300 kPa tensile stresses and 80 g vibratory accelerations	38
$NiCo_2O_4$/GF (Gyroid)	810 mF/cm^3	Asymmetric supercapacitor	Compressive stress: 1.4 MPa (GF substrate) Modulus: 12 MPa	/	67
PANI/C/SiOC (I-WP structure)	585.5 mF/cm^3 (3 mA/cm^3)	Symmetric supercapacitor	Compressive stress: 71.31 MPa Modulus: 2.72 GPa Energy absorption: 92.58 kJ/m3	Maintaining full functionality after impact (0.3 J/cm^3), under dynamic loading (0 to 18.83 MPa), and post electrolyte healing	This work

Detailed discussions of the comparison are included in the reivsed manuscript and the supplementary information: "Currently, efforts to develop 3D-printed PANI-based symmetric supercapacitors have

gradually enriched the existing body of research (Supplementary Table 1). However, their performance under complex conditions has rarely been explored[58-62]. The PANI/C/SiOC electrode not only demonstrated comparable capacitance to the 3D-printed PANI-based symmetric supercapacitors but also excelled due to its ability to operate under harsh conditions. In comparison with other rigid supercapacitor electrodes or cells, the Cell I-WP showed enhanced compressive strength and energy absorption, managing more practical yet extreme conditions with high damage invulnerability[38,63-67]. Future modifications of the PANI/C/SiOC supercapacitor should aim to enhance temperature adaptability, such as frost and drying resistance, thereby extending its application to more severe environments." (Page 28, lines 8-18)

"Increasing research has focused on fabricating 3D-printed structuralized supercapacitors using PANI and its composites as active materials, attributed to their distinctive electrochemical and physical properties. These components can serve as self-standing electrodes for theoretical electrochemical tests using a three-electrode system or be integrated into symmetric supercapacitors for practical performance evaluation. However, the functionality of usable 3D-printed PANI-based supercapacitor cells, particularly under complex working conditions, such as loading or after damage, remains less explored. This study enhances the load-bearing capability and damage invulnerability of the 3D-printed PANI-based supercapacitor cell by employing a ceramic-based current collector and self-healable hydrogel to assemble the cell. The resulting cell demonstrated compressive stress, Young's modulus, and energy absorption of 70.61 MPa, 2.75 GPa, and 92.15 kJ/m^3, (Specific compressive stress: 197.23 MPa, specific modulus: 7.68 GPa, specific energy absorption: 257.4 kJ/m^3), while maintaining capacitance comparable to that of reported symmetric supercapacitors, promising to extend the potential applications of PANI-based supercapacitors. Compared to other rigid supercapacitors or electrodes, the mechanical performance of Cell I-WP exhibited advantages due to the robust SiOC substrate. Furthermore, the cell's functionality was preserved under operational conditions post-impact (0.3 J/cm^3), under dynamic loading (0 to 18.83 MPa), and after electrolyte

healing, scenarios not typically covered in currently reported studies but crucial for practical applications. Given the use of PVA hydrogel, future research should focus on enhancing the temperature adaptability of the cell, such as resistance to frost and drying, thereby broadening its utility in harsher environments." (Supplementary information, Pages 15-16)

Reviewer #3

The authors described an impact-resistant and ready-to-use supercapacitors constructed from self-healable hydrogel electrolytes infused structurally reinforced lattice electrodes. The obtained supercapacitors exhibited good electrochemical performance with a static specific capacitance of 585.51 mF/cm3 at a current density of 3 mA/cm3. It maintained operational integrity under extreme conditions, including post-impact with energy of 0.3 J/cm^3, dynamic loading ranging from 0 to 18.83 MPa, and self-healing after electrolyte damage. This approach provides a facile strategy for creating damage-invulnerable energy storage devices. The approach is systematic and the quality of the presentation in the manuscript is very good. However, the following points should be addressed before the manuscript can be accepted for publication.

1. The introduction states that "Supercapacitors, as burgeoning storage devices, are no exception. Their rapid charge-discharge rates make them apt for extreme environments". The logical correlation between the rapid charge-discharge rates of supercapacitors and their applicability to extreme environments is puzzling. It is therefore recommended that more precise wording be used.

Response: Thank you very much for your meticulous guidance and suggestions. In certain applications, such as engine ignition systems in rockets, missiles, and aircraft, supercapacitors are frequently utilized for their high instantaneous power. The working conditions for these applications are usually harsh, requiring that supercapacitors maintain functionality throughout storage, transportation, and operation. We aim to underscore such application context of these supercapacitor devices to elucidate the motivation of the designs in this work. Following your recommendation, we have added further

explanations to clarify any ambiguities: "Their rapid charge-discharge rates render them suitable for extreme environments, such as engine ignition systems that require high instantaneous power, demanding high working stability and damage resistance." (Page 2, lines 13-16)

2. A clearer description of the innovation of the study is suggested in the introduction section.

Response: We appreciate the reviewer for the comments! Our work aims to develop a strategy for creating comprehensive, tailored, damage-resistant, and ready-to-use supercapacitors by employing 3D-printed ceramics-based electrodes paired with self-healable hydrogel electrolytes. To further underscore the innovative aspects, additional discussions on the motivation have been included:

"Since electrodes are typically engineered into specific configurations and dimensions to fully utilize their electrochemical and mechanical performance in device assemblies, a further significant advantage of SiOC substrates is their compatibility with 3D printing techniques for flexible configuration design. This adaptability facilitates the optimal use of confined spaces by electrode architecture adjustment, maximizing active material load and minimizing weight, thereby reducing energy self-consumption, while fine-tuning the mechanical properties[23-25]." (Page 3, lines 13-20)

"Meanwhile, rigid and impact-resistant supercapacitors are also essential in specific applications such as aerospace, underwater equipment, and new energy vehicles[38]. Consequently, enhancing hydrogel supercapacitors with 3D-printed SiOC lattice-based electrodes holds promise for broadening their application scope." (Page 4, lines 14-18)

"The assembly strategy of the supercapacitor cell is also crucial to mechanical stability. Given that supercapacitors employ an "electrode-electrolyte-electrode" configuration, they are typically constructed using lamellar structures. This arrangement may introduce mechanical weak points determined by the least robust component within the structure and induce anisotropy in mechanical behavior. To develop a mechanically coherent and isotropic supercapacitor cell, we employed a

continuous all-SiOC-based skeleton to enhance mechanical performance uniformly. Triply periodic minimal surface (TPMS) configurations were used to construct the SiOC skeleton, leveraging their structural uniformity and periodicity. Electrodes were fabricated via in-situ growth of active materials on the TPMS-structured SiOC, paired with an insulating SiOC separator that shared the same TPMS design. The hydrogel electrolyte was infused into the hollow spaces to complete a hydrogel-infused TPMS lattice configuration as a ready-to-use supercapacitor cell. Since this design was reinforced by the continuous SiOC skeleton, weak phases and anisotropic mechanical behavior common in lamellar or sandwich structures can be avoided. This uniform continuity and periodicity between the electrode and separator allowed the skeleton to distribute stress evenly, mitigating stress concentration. Furthermore, the employment of scalable and customizable 3D printing techniques endowed this strategy with the potential for creating comprehensive, tailored, damage-resistant, and ready-to-use supercapacitors." (Page 5, lines 3-22)

This work is further compared with those of recently reported 3D-printed PANI supercapacitors and rigid supercapacitors in Supplementary Table 1, to emphasize its distinctiveness and practical utility

Supplementary Table 1. Comparison of the recently reported 3D-printed PANI supercapacitors and rigid supercapacitors.

Electrode (Structure)	Specific capacitance	Measurement	Mechanical performance	Damage resistance	Ref
PANI/Fe-Ni (Scaffold)	540.68 F/g (5 mV/s)	Two-electrode system	/	/	58
MnO_2/PANI (Interdigital structure)	575 F/g (0.4 A/g)	Asymmetric supercapacitor	/	/	59
PANI hydrogel (Printable)	422 F/g (0.2 A/g)	Three-electrode system	/	/	60
Graphene/ PANI (Mesh)	483.9 mF/cm^2 (0.5 mA/cm^2)	Symmetric supercapacitor	/	/	61
PANI/RGO (Interdigital structure)	1329 mF/cm^2 (5 mA/cm^2)	Symmetric supercapacitor	/	/	62
Porous carbon (Microlattice)	105 F/g	Three-electrode system	Compressive stress: ~10.45 MPa Modulus: 0.74 Gpa	/	63
$Cu(OH)_2$/Cu/Ceramic (Octet-truss lattice)	831 F/g (5 mA/cm^3)	Three-electrode system	Specific compressive stress: 30.02 MPa Specific energy absorption: 264.7 kJ/m^3	/	64
Ti_3C_2Tx-MXene/resin (Octet structure)	74 F/g (30 mV/s)	Three-electrode system	Compressive stress: ~12.5 MPa Modulus: 0.15 Gpa	/	65
(Ni, Co, Mn) Se/Carbon-rich lattices (Wave structure)	7.8 F/cm^2 (1 mA/cm^2)	Three-electrode system	Specific compressive stress: 9.52 MPa Specific modulus: 0.26 GPa Specific energy absorption: 18.33 kJ/m^3	Maintaining 60% capacitance after 5000 cycles under 3 MPa at 85 °C	66
Porous silicon (Plate)	20 Wh/kg	Symmetric supercapacitor	Tensile strength: 300 kPa Shear strength: 120 kPa	Maintaining 10 W h/kg under 300 kPa tensile stresses and 80 g vibratory accelerations	38
$NiCo_2O_4$/GF (Gyroid)	810 mF/cm^3	Asymmetric supercapacitor	Compressive stress: 1.4 MPa (GF substrate) Modulus: 12 MPa	/	67
PANI/C/SiOC (I-WP structure)	585.5 mF/cm^3 (3 mA/cm^3)	Symmetric supercapacitor	Compressive stress: 71.31 MPa Modulus: 2.72 GPa Energy absorption: 92.58 kJ/m3	Maintaining full functionality after impact (0.3 J/cm^3), under dynamic loading (0 to 18.83 MPa), and post electrolyte healing	This work

Detailed discussions of the comparison are included in the reivsed manuscript and the supplementary information: "Currently, efforts to develop 3D-printed PANI-based symmetric supercapacitors have

gradually enriched the existing body of research (Supplementary Table 1). However, their performance under complex conditions has rarely been explored[58-62]. The PANI/C/SiOC electrode not only demonstrated comparable capacitance to the 3D-printed PANI-based symmetric supercapacitors but also excelled due to its ability to operate under harsh conditions. In comparison with other rigid supercapacitor electrodes or cells, the Cell I-WP showed enhanced compressive strength and energy absorption, managing more practical yet extreme conditions with high damage invulnerability[38,63-67]. Future modifications of the PANI/C/SiOC supercapacitor should aim to enhance temperature adaptability, such as frost and drying resistance, thereby extending its application to more severe environments." (Page 28, lines 8-18)

"Increasing research has focused on fabricating 3D-printed structuralized supercapacitors using PANI and its composites as active materials, attributed to their distinctive electrochemical and physical properties. These components can serve as self-standing electrodes for theoretical electrochemical tests using a three-electrode system or be integrated into symmetric supercapacitors for practical performance evaluation. However, the functionality of usable 3D-printed PANI-based supercapacitor cells, particularly under complex working conditions, such as loading or after damage, remains less explored. This study enhances the load-bearing capability and damage invulnerability of the 3D-printed PANI-based supercapacitor cell by employing a ceramic-based current collector and self-healable hydrogel to assemble the cell. The resulting cell demonstrated compressive stress, Young's modulus, and energy absorption of 70.61 MPa, 2.75 GPa, and 92.15 kJ/m^3, (Specific compressive stress: 197.23 MPa, specific modulus: 7.68 GPa, specific energy absorption: 257.4 kJ/m^3), while maintaining capacitance comparable to that of reported symmetric supercapacitors, promising to extend the potential applications of PANI-based supercapacitors. Compared to other rigid supercapacitors or electrodes, the mechanical performance of Cell I-WP exhibited advantages due to the robust SiOC substrate. Furthermore, the cell's functionality was preserved under operational conditions post-impact (0.3 J/cm^3), under dynamic loading (0 to 18.83 MPa), and after electrolyte

healing, scenarios not typically covered in currently reported studies but crucial for practical applications. Given the use of PVA hydrogel, future research should focus on enhancing the temperature adaptability of the cell, such as resistance to frost and drying, thereby broadening its utility in harsher environments." (Supplementary information, Pages 15-16)

3. Some data should be measured several times and given as mean ± standard deviation, e.g. mechanical properties and conductivity.

Response: Thank you for pointing this out! The mechanical properties, density, and conductivity measurements have been taken on 5 different samples.To ensure data accuracy, the average values with corresponding error bars (standard deviation) have been reported.:

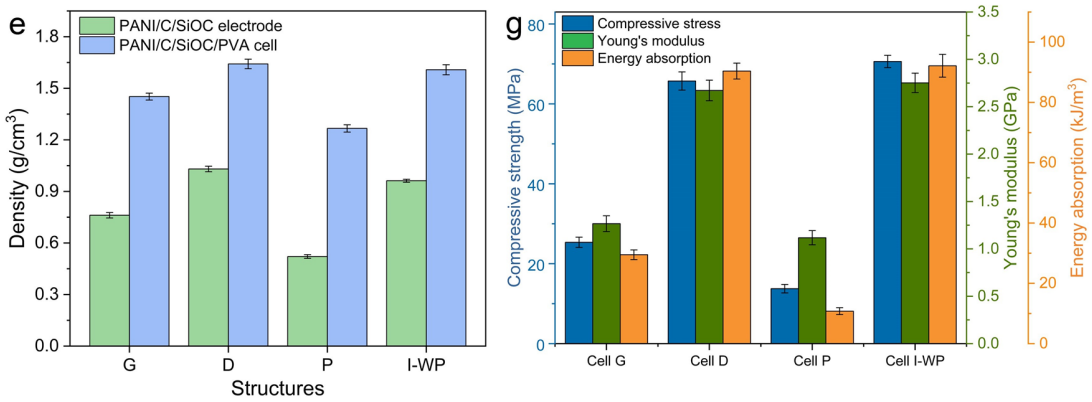

Fig. 1 Schematics of the hydrogel-infused lattice supercapacitor and mechanical performance: (e) Density of the PANI/C/SiOC electrodes and PANI/C/SiOC cells; (g) Compressive stress, Young's modulus, and energy absorption values of PANI/C/SiOC cells with different TPMS structures.

"The resulting cells exhibited impressive lightness which can be attributed to the low densities of both the electrodes and the electrolyte. The densities for the electrodes G, I-WP, D, and P were measured at 0.76 ± 0.016, 0.96 ± 0.008, 1.03 ± 0.015, and 0.52 ± 0.011 g/cm^3, respectively, indicating the lightness and high process stability. The assembled cells exhibited a slight increase in density due the infusion of hydrogel electroltyte, ranging from 1.27 to 1.64 g/cm^3 (Fig. 1e)." (Page 10, lines 11-16)

"The cells, designed with G, D, P, and I-WP structures, demonstrated compressive stresses of 25.36 ± 1.27, 65.72 ± 2.28, 14.75 ± 1.06, and 70.61 ± 1.53 MPa, respectively, along with corresponding energy absorption capacities of 29.49 ± 1.59, 90.40 ± 2.65, 10.76 ± 1.14, and 92.15 ± 3.78 kJ/m^3 (Fig. 1g)." (Page 11, lines 4-9)

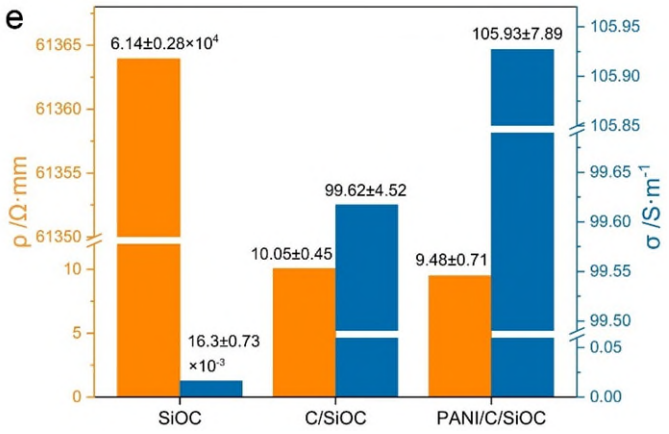

Fig. 2 Characterization of C/SiOC current collector: (e) Conductivity of SiOC, C/SiOC, and PANI/C/SiOC

"The resistivity and conductivity of pristine SiOC were measured as 6.14 ± 0.28×10^4 Ω·mm and 16.3 ± 0.73×10^{-3} S/m, respectively, while those of C/SiOC reaching 10.05 ± 0.45 Ω·mm and 99.62 ± 4.52 S/m, respectively (Fig. 2e)." (Page 13, lines 8-12)

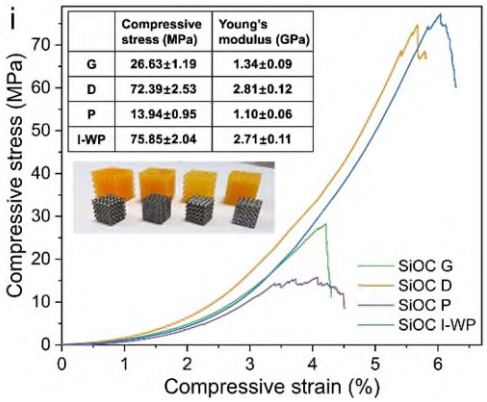

	Compressive stress (MPa)	Young's modulus (GPa)
G	26.63±1.19	1.34±0.09
D	72.39±2.53	2.81±0.12
P	13.94±0.95	1.10±0.06
I-WP	75.85±2.04	2.71±0.11

Fig. 4 Electrochemical performance post impact and under dynamic pressure loading: (i) Compressive stress curves of SiOC substrates with TPMS structures

"The SiOC substrate with G, D, P, and I-WP structures exhibited compressive strength of 26.63 ± 1.19, 72.39 ± 2.53, 13.94 ± 0.95, and 75.85 ± 2.04 MPa, respectively, and corresponding Young's modulus of 1.34 ± 0.09, 2.81 ± 0.12, 1.10 ± 0.06, and 2.71 ± 0.11 GPa (Fig. 4i)." (Page 22, line 15-18)

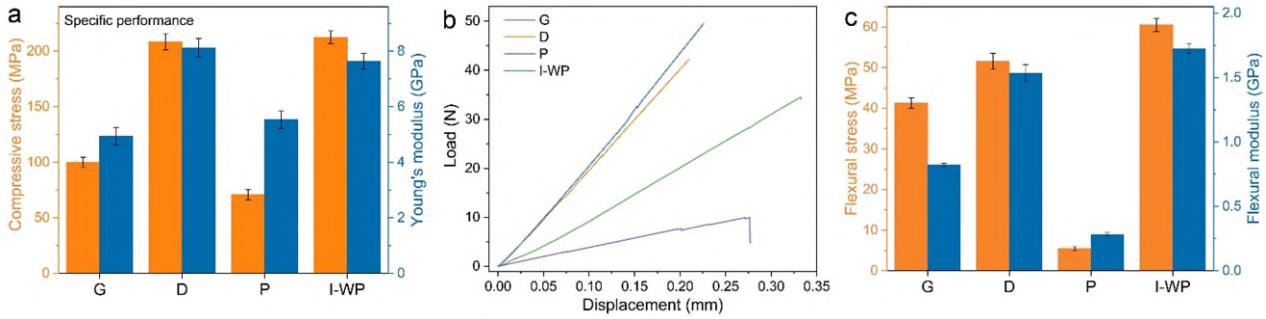

Supplementary Fig. 11 Mehcanical performance of C/SiOC current collector. (a) Specific compressive stress and Young's modulus of SiOC substrates with different structures. (b) Three-point bending performance of the SiOC substrates with different structures and (c) corrrsponding flexural stress and modulus.

"The C/SiOC current collector with G, D, P, and I-WP configurations exhibited specific compressive stresses of 99.96 ± 4.43, 208.41 ± 7.26, 70.96 ± 4.76, and 212.42 ± 5.71 MPa, respectively, with the corresponding specific modulus of 4.94 ± 0.32, 8.12 ± 0.33, 5.54 ± 0.32, 7.63 ± 0.28 GPa (Supplementary Fig. 11a)." (Supplementary information, pages 10, lines 8-11)

"Flexural stresses for the cells with G, P, D, and I-WP configurations were 41.24 ± 1.29, 51.54 ± 1.97, 5.49 ± 0.44, and 60.54 ± 1.62 MPa, respectively. Concurrently, the corresponding modulus were 0.83 ± 0.012, 1.53 ± 0.066, 0.28 ± 0.013, and 1.73 ± 0.039 GPa (Supplementary Fig. 11c), corroborating the inherently robust mechanical attributes of the current collectors." (Supplementary information, pages 10, lines 16-20)

4. The hydrogel electrolyte adheres to the electrode by in situ molding. Is it possible that mechanical interlocking due to the configuration design of the electrodes also contributes to the adhesion? This should be clarified.

Response: We are grateful for your valuable suggestion. Mechanical interlocking can be incorporated into the electrode design to improve adhesion and assembly. A conventional electrode shape was used in this for the standardization in measuring and calculating theoretical performance. In the revised manuscript, we designed and fabricated an interlocked cell to demonstrate the flexibility of design and assembly. Illustrations have been added to aid in clarification: "Another advantage of 3D printing lies in its flexibility in cell architecture design. Although this work employed a conventional electrode shape to standardize the calculation and evaluation of theoretical performance, the further design of seamless joints between electrodes and separators is straightforward and adaptable. The design of interlocking structures can offer a diverse assembly approach (as illustrated in Fig. 5i), enabling the creation of customized and stable devices tailored to various application requirements with firmer and more robust assembly manners." (Pages 28-29)

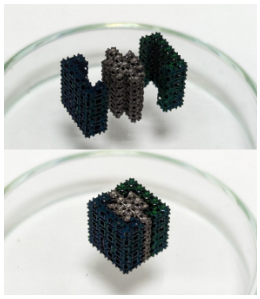

Fig. 5 Self-healing performance of PVA hedrogel and scalability of the cells: Photography showing the (i) interlocking structure of the cell.

5. The mechanical properties of the SIOC without surface-configuration design and its electrochemical performance after assembly into supercapacitors should be given for presenting the advantages of this work.

Response: Many thanks for the valuable comment! The electrochemical performance of supercapacitors using PANI/C/SiOC and C/SiOC electrodes without specific surface-configuration designs was tested and compared to that of TPMS-structured electrodes to highlight their advantages:

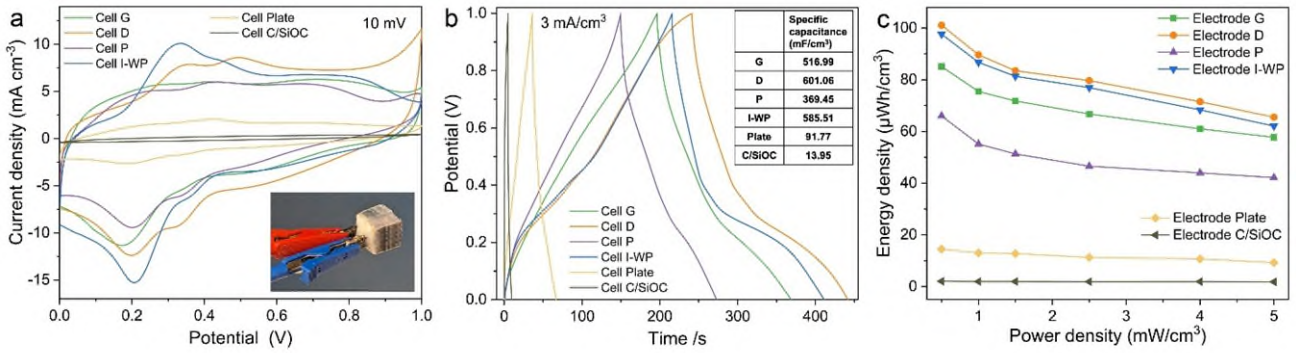

Fig. 3 Electrochemical properties and characterization of PANI/C/SiOC cells: Electrochemical properties of cell with different electrode structures: (a) CV curves, (b) GCD curves, and (c) Ragone plots (power density vs energy density)

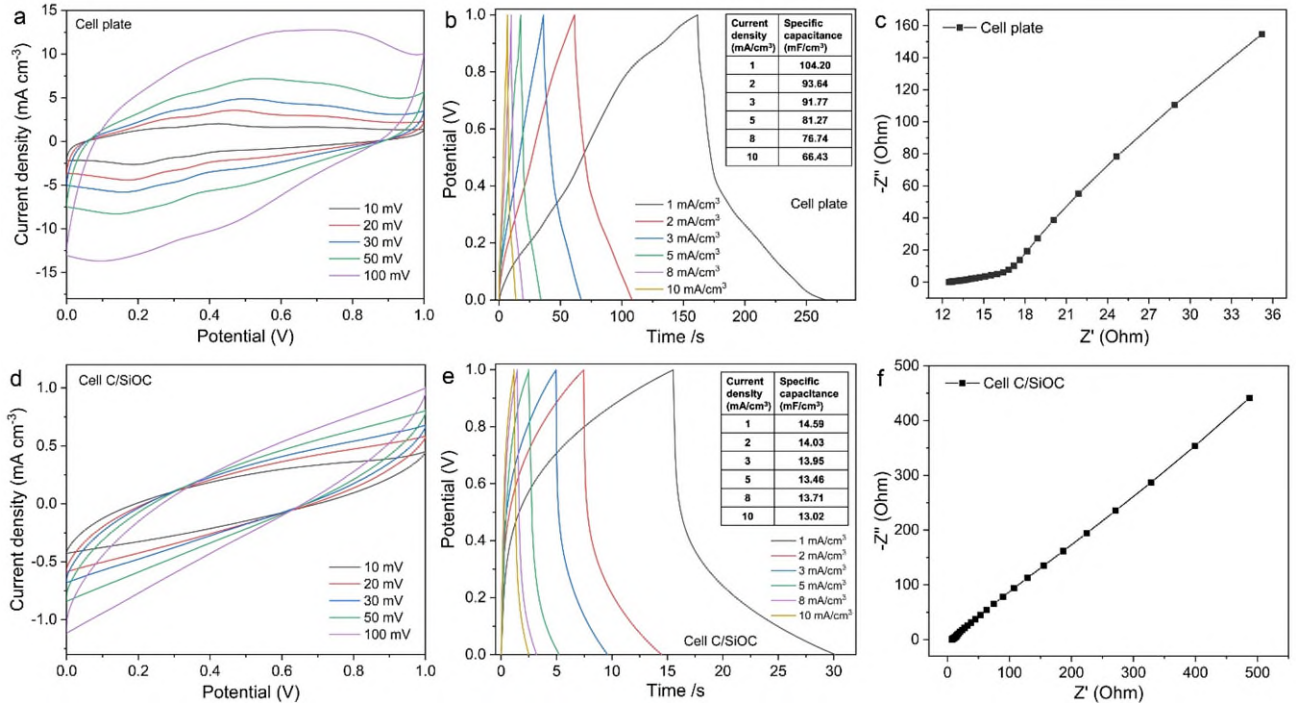

Supplementary Fig. 4 Electrochemical performance of Cell with PANI/C/SiOC and C/SiOC plates as electrodes: (a) CV curves, (b) GCD curves, and (c) EIS plots of Cell plate. (d) CV curves, (e) GCD curves, and (f) EIS plots of Cell C/SiOC.

Detailed discussions of these comparison are included in the reivsed manuscript and the supplementary information: "Cyclic voltammetry (CV) analysis, conducted at a scan rate of 10 mV/s, revealed that electrodes with solid plate structure and varying TPMS structures exhibited similar redox peaks (Fig. 3a)." "Furthermore, the CV curves of the C/SiOC current collector exhibited no redox peaks, indicating that the pseudocapacitive reactions occurred mainly on the PANI active layer (Supplementary Fig. 4)." (Page 14, lines 10-20)

"Specific capacitances for the G, D, P, and I-WP structured electrodes were calculated at 516.99, 601.06, 369.45, and 585.51 mF/cm^3, respectively, indicating an enhancement when compared to the PANI/C/SiOC electrode (91.77 mF/cm^3) and the solid plate structured C/SiOC current collector (13.95 mF/cm^3, Supplementary Fig. 4)." (Page 16, lines 15-19)

"Supplementary Fig. 4 presents the electrochemical performance of cells with PANI/C/SiOC plate electrodes (Cell plate) and C/SiOC plate electrodes (Cell SiOC). The CV curves (10-100 mV/s) of the Cell plate exhibited redox peaks similar to those of the cell using TMPS-structured electrodes, suggesting that the electrode architecture hardly affected the pseudocapacitive reactions. The GCD (1-10 mA/cm^3)curves also displayed shapes similar to those of other TMPS-structured electrodes, resembling isosceles triangles. However, TMPS structured electrodes demonstrated enhanced specific capacitance compared to the PANI/C/SiOC plate electrodes, attributable to the increased surface area that accommodated a larger PANI layer. Conversely, the CV curves of the Cell C/SiOC showed no redox peaks, confirming that the pseudocapacitive reactions scarcely involved the C/SiOC current collector. Nonetheless, the Cell C/SiOC still exhibited little energy storage capacity with a specific capacitance of approximately 14 mF/cm^3 at different current density, primarily due to its electric double-layer capacitance characteristics, which minimally contributed to the overall capacitance of the TMPS structured cells." (Supplementary information, page 4)

The mechanical properties of SiOC without surface configuration are then evaluated. However, these properties did not meet expectations, primarily due to cracks and defects generated by the pyrolysis of polymeric precursors, which is a typical issue for bulk polymer-derived ceramics. This can be mitigated by incorporating hollow structures. Consequently, data on the mechanical properties of solid SiOC have been included, and the necessity and advantages of creating TPMS structures are discussed:

"It is important to note that the creation of hollow structures within SiOC ceramics can effectively mitigate the formation of cracks and pores resulting from the pyrolysis of bulk polymeric precursors[18,20]. The compressive stress curve of solid SiOC indicated multiple peaks indicative of structural flaws and registered a compressive strength of 46.79 ± 5.6 MPa, with a higher standard deviation compared to those of TPMS-structured SiOC due to the defects (Supplementary Fig. 10). In contrast, the I-WP structured SiOC demonstrated a more uniform stress distribution with enhanced compressive strength, revealing that this configuration not only reduced weight and increased surface area, but also optimized mechanical behavior." (Pages 22-23)

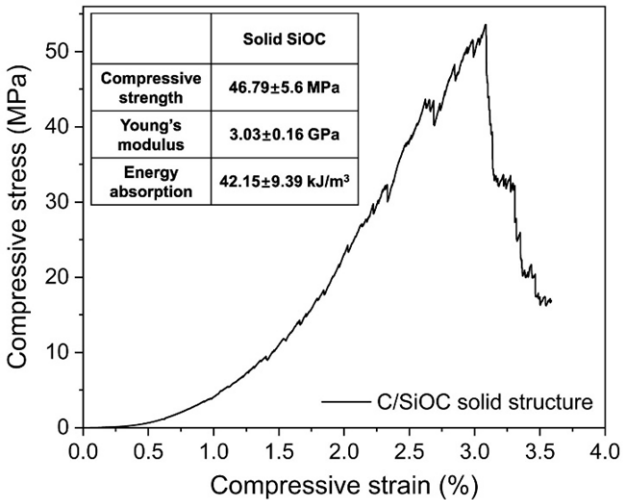

Supplementary Fig. 10 Compressive stress curve of solid SiOC.

"Supplementary Figure 10 displays the compressive stress curve of solid SiOC, which exhibits multiple peaks due to defects formed during pyrolysis, resulting in stress fluctuations. Consequently, solid SiOC did not demonstrate excellent mechanical behavior as expected. Its compressive strength,

Young's modulus, and energy absorption measured 46.79 ± 5.6 MPa, 3.03 ± 0.16 GPa, and 42.15 ± 9.39 MPa, respectively. This is a typical issue for bulk polymer-derived ceramics (PDC), which can be mitigated by incorporating hollow structures within the PDC. Therefore, the creation of TPMS structures within SiOC proved to be an effective method to optimize its mechanical performance." (Supplementary information, pages 9)

6. Why do Cell G and Cell P in Fig. 3g show differences in charging and discharging behavior with Cell D and Cell I-WP in the mid-charging and late discharging stages?

Response: We highly appreciate the reviewer for pointing this out! The observed differences in charging and discharging behavior can be attributed to the varying active areas of each electrode, which affected the engagement effectiveness of PANI in the redox processes. Although the measurements were conducted under the same volumetric charging and discharging current densities, the area-specific current densities differed due to the varying surface areas of each electrode. Consequently, the G and P structured electrodes, which actually operated at higher area-specific current densities, exhibited less effective engagement of PANI in the redox processes due to inadequate faradaic redox kinetics and less pronounced charging and discharging plateaus. Additional explanations have been included in the revised manuscript to clarify this phenomenon: "However, the electrodes with D and I-WP structures exhibited more pronounced charging and discharging plateaus, attributable to more efficient redox processes. Despite each electrode operating at the same volumetric charging and discharging current density, variations in active material loading (stemming from differences in the specific surface areas of each electrode) resulted in differing area-specific charging and discharging current densities. Consequently, the G and P structured electrodes were operated at higher area-specific current densities, leading to less effective engagement of PANI in the redox processes due to inadequate faradaic redox kinetics. Therefore, it can be concluded that while all electrodes can operate

at high current densities, those with a higher specific surface area can develop a larger active layer, thereby facilitating more sufficient redox processes and maximizing the electrochemical performance of the active layer." (Page 16, line 4-22)

7. Abbreviations appear directly in some words, e.g., XPS, which authors are asked to double-check and revise.

Response: Thank you very much for your careful review of the manuscript! We apologize for the oversight. We have reviewed the manuscript and defined the previously omitted abbreviations at their first occurrence: "TPMS SiOC was then coated by pyrolytic carbon (C/SiOC)" (Page 6, line 8), "Scanning electron microscope (SEM)" (Page 11, lines 19-20), "X-ray photoelectron spectroscopy (XPS)" (Page 12, line 20), "Fourier-transform infrared spectroscopy (FT-IR)" (Page 18, line 1), "electrochemical impedance spectroscopy (EIS)" (Page 20, line 15), "High resolution transmissione electron microscope (HRTEM)" (Page 21, lines 9-10). Additionally, we have double-checked the manuscript to eliminate any further writing and formatting errors. All revisions are highlighted in red for ease of review.

We extend our gratitude once again for your constructive comments and suggestions, which have been instrumental in guiding us to refine and enhance the quality of our manuscript. We hope that the revisions made meet your expectations. Should there be any further queries or requirements for additional modifications, we remain fully prepared to undertake further revisions.

Sincerely,

Ding Jun

REVIEWERS' COMMENTS

Reviewer #1 (Remarks to the Author):

The authors have answered all my questions, and I would recommend accepting it as is.

Reviewer #2 (Remarks to the Author):

Authors correctly answered on all reviewer questions and suggestions, so the paper could be accepted.

Reviewer #3 (Remarks to the Author):

Initial comments have been responded to and resolved.